Zootaxa 4052 (2): 151–179
www.mapress.com/zootaxa/

Article

ISSN 1175-5326 (print edition)
ZOOTAXA
ISSN 1175-5334 (online edition)

http://dx.doi.org/10.11646/zootaxa.4052.2.1
http://zoobank.org/urn:lsid:zoobank.org:pub:3D92BEC3-F344-470F-AE21-94978465F1EA

Holistic morphometric analysis of growth of the sand dollar *Echinarachnius parma* (Echinodermata:Echinoidea:Clypeasteroida)

LOUIS G. ZACHOS
Department of Geology and Geological Engineering, University of Mississippi, University, MS 38677, USA.
E-mail: lgzachos@olemiss.edu

Abstract

Holistic morphometrics is a term implying complete shape characterization of all of the structural parts of an organism. The skeleton of an echinoid is comprised of hundreds of individual plates arranged in a closed 3-dimensional mosaic forming the test. GIS software and techniques were used to generate topologically correct digital models of an ontogenetic series of specimens of the sand dollar echinoid *Echinarachnius parma*. Plate growth can be considered in proportion to overall skeleton growth, resulting in a linear model of relative growth. Alternatively, separate logistic equations can be fit to the ontogenetic series of homologous plate areas using nonlinear least squares regression to result in a model for instantaneous growth. The linear and logistic parameters of the models describe the allometric growth of plates from different viewpoints. Growth is shown to fall into characteristic patterns defining distinct plate growth domains associated with development of the imago (larval) skeleton just prior to metamorphosis, early growth associated with expansion of the corona and fold-over (forming the flattened body form), juvenile growth and formation of petals, and adult growth. Functions of growth, plate translocation, plate juxtaposition between aboral and oral surfaces, and relationships with internal buttressing are quantified. Results offer explanations for general skeletal symmetry, distinction between ambulacral and interambulacral growth, the relationship of growth to internal buttressing, existence of a distinct petalodium, and anterior-posterior asymmetry during development. The parametric values of growth functions derived from the results are a basis for computational modeling of growth and development in sand dollars.

Key words: Skeleton, GIS, morphology, ontogeny, allometry, computational model

Introduction

The skeleton or test of the sand dollar echinoid *Echinarachnius parma* shows nearly symmetrical growth, with simple petals (flush, lacking demiplates or occluded plates) and no lunules. These characteristics make the species an ideal model for a study of growth and development of the skeleton. At metamorphosis, the skeleton of *E. parma* may have as few as 38 plates, but as a fully mature adult the number can exceed 1000 plates. The flattened form of sand dollars results in a restricted number of plates (about 100) on the ventral or oral side, so that nearly all plates are added to the dorsal or aboral side. Growth of the animal requires growth of the individual plates concomitant with addition of new plates within constraints of overall body form. This study uses a holistic approach to incorporate measurements of plate growth throughout ontogeny from juvenile through mature adult stages, based on detailed measurements of dimension and location of all of the plates for all specimens in the series. Plate homology among individuals is based on plate cohort number. The set of basicoronal plates (those surrounding the peristome) are the first cohort and cohort number increases monotonically for plates in each of the 20 columns. Plate growth can be considered in proportion to overall skeleton growth, resulting in a linear model of growth. Alternatively, separate logistic equations can be fit to the ontogenetic series of homologous plate areas using nonlinear least squares regression. The logistic and linear coefficients describe the allometric growth of plates from different viewpoints, and growth is shown to fall into characteristic patterns defining distinct plate growth domains. Major stages of development can be divided into development of the imago skeleton just prior to metamorphosis, early growth associated with expansion of the corona and fold-over (forming the flattened body form), juvenile

Accepted by M. Eleaume: 2 Nov. 2015; published: 2 Dec. 2015

growth and formation of petals, and adult growth. The beginning of each of these stages represents a significant change in developmental trajectory as measured by growth parameters. It is expected that even minor variation in the relative timing of these stages (heterochrony) can lead to significant variation in morphogenesis and phenotypic expression. By the empirical determination of parametric equations of plate growth this study is the basis for continuing work on modeling development in echinoids.

Material and methods

Specimens of *E. parma* were collected from Mowry Beach (on the Bay of Fundy) at Lubec, Maine over 2 summers. Tidal range at this locality averages about 6.5 meters, and living specimens from about 2mm to 75mm diameter (Figure 1) were collected from shallow water at low tides. Smallest juveniles were found in mid to late July, coincidental with spring tides at dawn. Collections were restricted to this one area to minimize variations attributable to differences between populations.

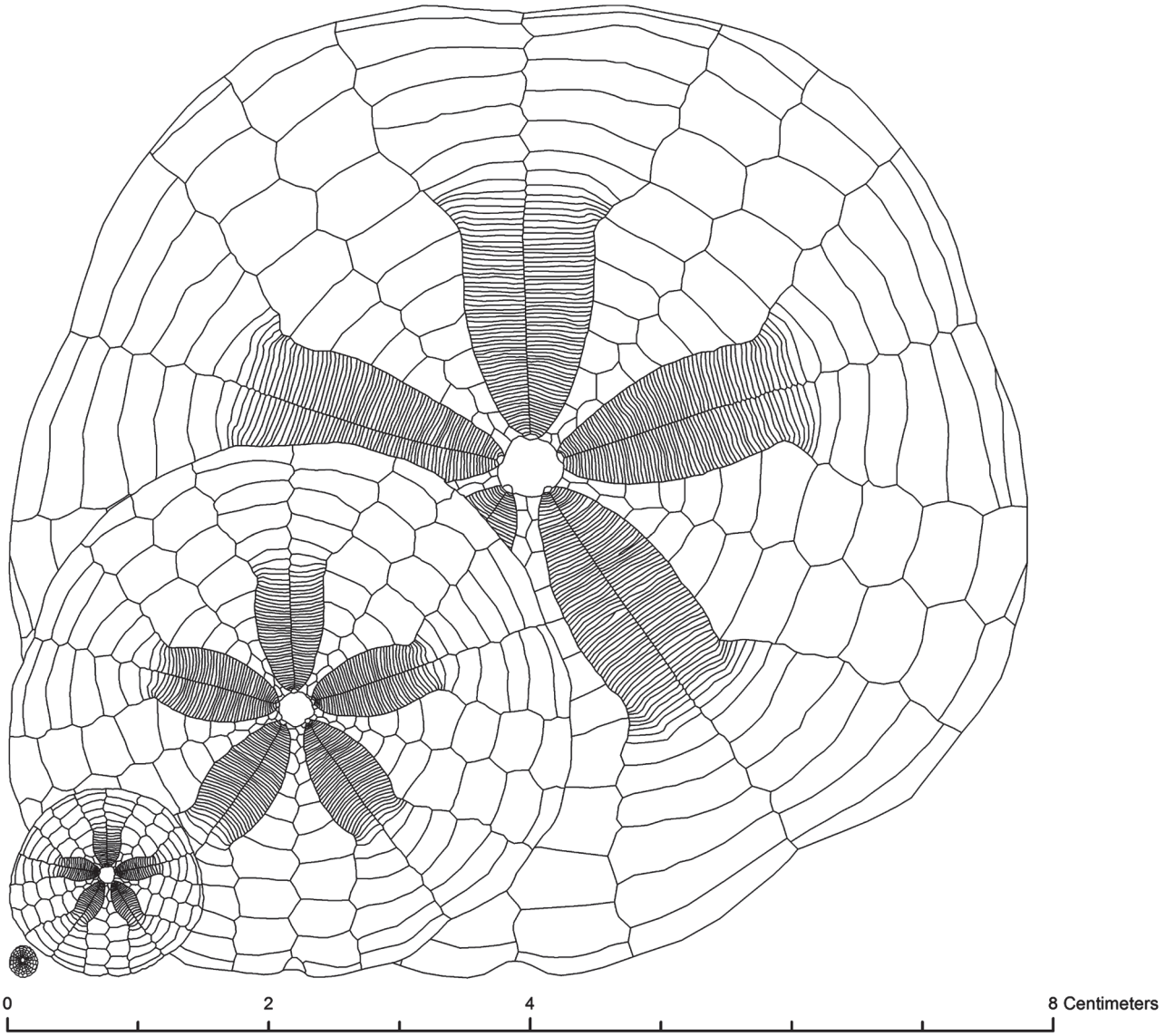

FIGURE 1. Plate diagrams of *Echinarachnius parma* showing the range of sizes attained during growth. Length of smallest specimen 2.45mm, length of largest 75mm.

A mature individual of *E. parma* has a skeleton composed of approximately 1000 individual calcite plates (the largest specimen described here had 1072 plates). All of the plates of selected and cleaned individual specimens

were manually digitized from scaled photographs and converted into topologically correct polygons using ArcGIS®. These polygons were labeled by plate type and indexed using an echinoid-centric numbering system. This permitted the determination of plate cohorts and allows not only static measurement of plate location and dimension, but also the ability to map the changes in size and relative position during growth. A MorphoBank project (#2276) was created as a data repository of the GIS data files, including a file geodatabase, exported shapefiles, map files, and imagery (Zachos 2015).

Coronal plates were numbered sequentially in columns with the basicoronal set of plates beginning at 1 and ascending towards the apical system. Columns were labeled traditionally using the Lovén system (Lovén 1874) of Roman numerals for ambulacral columns and Arabic numerals for the interambulacral columns, left and right half-columns denoted by the letters a and b, ordered in a clockwise direction when viewed from the oral side. **However, for the purposes of this study, the point of view is always from the dorsal side for both aboral and oral views (i.e., the oral plates are mirrored from their traditional view).** In this case, the columns are ordered in a counter-clockwise direction for both aboral and oral surfaces, and plate patterns can be directly overlaid.

Marginal plating is difficult to delineate strictly from an exterior view. The margin can be shown to consist of 2 to 4 independent plates (Seilacher 1979; Seilacher & Gishlick 2015). An inability to account for the plate numbers in the margin can result in mismatch of cohort numbers for aboral plating. However, evidence indicates that the independent plates in the margin arose from partitioning of existing plates, and therefore does not affect the numbering of cohorts. This is confirmed by (a) the lack of specific marginal plates in the imago (b) similar partitioning of existing plates following margin damage, and (c) consistent cohort patterning irrespective of the number of marginal plates. Notable teratologies support the hypothesis that plates can split. An example is shown in Figure 2A, where damage to the anterior portion of the test has resulted in splitting of several plates near the margin (this specimen was collected alive, confirming that it had survived the trauma and repaired the margin). Although no juveniles smaller than 2mm length were examined in this study, Gordon (1929) showed that just post-metamorphosis (when the length was 0.52mm) there are 4 plates in interambulacrum 5 posterior to the periproct, which itself abuts directly against the genital plate. In several juveniles 2.4mm to 2.5mm in length there are 3 plates completely oral, and the fourth plates begin orally and abut the peristome aborally. No additional plates can possibly be inserted on the margin between the periproct and the oral surface, yet in larger juveniles and adults there are as many as 3 marginal plates. These correspond exactly to the additional marginal plates in the other interambulacra.

In the smallest juveniles (<3mm length) there is a single plate that forms the margin in each interambulacral column. This is confirmed by the early formation of internal walls of stereom (which eventually become part of the internal buttressing system). Walls begin to form from 3 plates on the interradius in each interambulacrum – the marginal plate and the two adjacent inframarginal plates (Figure 2B). In adult specimens, there are 3 or 4 plates on the margin instead of the one original (Figure 2C). Thin sections of the margin show a variation in extinction angles under polarized light that indicates that the original single marginal plate was split or partitioned into multiple plates (Figure 2D). In some cases, the optical properties suggest an intermediate stage in which part of the marginal plate remains in continuity while part is split (Figure 2E). Marginal ambulacral plates (which are the same size as interambulacral marginal plates in juveniles) show the same pattern, except there is no formation of a radial buttress wall. The alternating plate offset pattern is maintained around the margin. Aboral plate cohort number, therefore, is considered to continue in sequence from the number of the last oral plate if more than ¼ the area of the alternate aboral plate or the number of the last oral plate plus 1 otherwise, constrained to continue the alternating plate pattern in each column.

Age estimation

Because specimens were collected from the wild their age was undetermined. An estimate of age can be made by counting growth bands in the individual plates. Unfortunately, the most common method of preparation (charring and immersion in xylene) is destructive. Another method that often but not always revealed growth bands was staining with food dyes containing FD&C Blue No. 1 (erioglaucine) dissolved in ethanol (Figure 3). Although counting growth lines can be used to estimate the age of a medium size test, it is not a reliable method for very small or very large specimens (Ebert 2013).

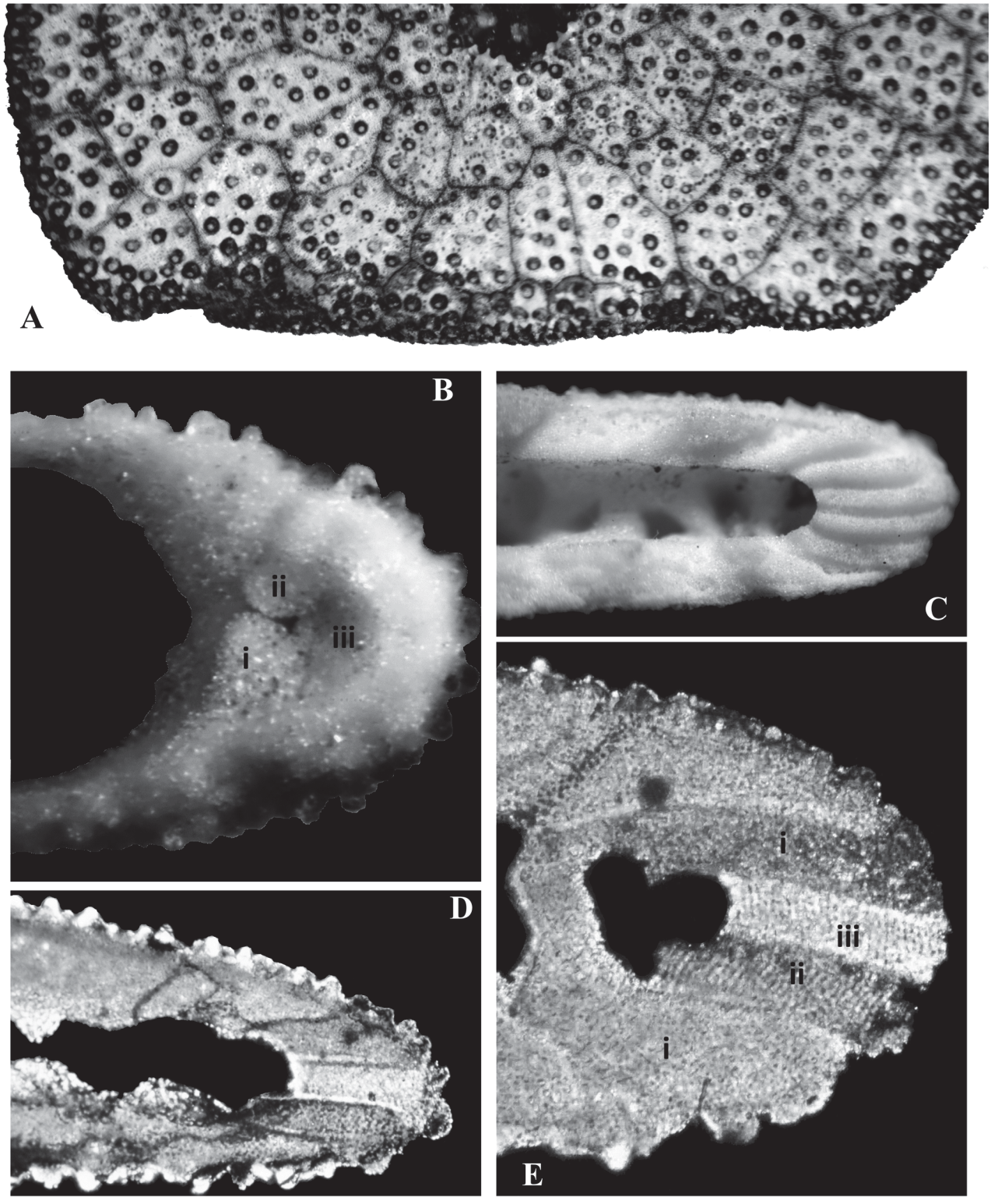

FIGURE 2. Evidence for splitting of marginal plates during ontogeny. A. Edge of injured specimen showing splitting of the marginal plates during repair. B. Interradius of interambulacral margin of specimen approximately 3mm in length showing early formation of buttress walls, one (iii) from a single marginal plate and the other two (i and ii) from adjacent inframarginal plates. C. Margin separated along the perradial suture showing four marginal plates. D. Thin section of interambulacral margin with crossed polars showing three split plates. E. Thin section of ambulacral margin showing two marginal plates (ii and iii) embedded within an optically continuous third marginal plate (i).

Brown (1983) did not report any sexual dimorphism in *E. parma*, although sex determination was not possible below a test length of 43mm. He showed that weight increased logarithmically as a function of length. Steimle (1990) found that growth curves of mean width for *E. parma* were sigmoidal, i.e. logistic, with specimens reaching a maximum width of about 40mm in 5–6 years. Hamel & Himmelman (1992) demonstrated sexual dimorphism expressed as oral surface concavity amounting to 8 to 14% difference in volume between males and females. Cabanac & Himmelman (1996) showed a logistic growth curve based on the Richards function (Richards 1959) derived empirically from a population of *E. parma*. Their studied population reached a maximum diameter of 60mm at an age of 11–12 years (attaining sexual maturity at 28mm at about 7 years). One prepared specimen from this study with a length of 59mm had 5 dark growth rings (Figure 3), indicative of an age of 5–6 years, leaving little doubt that the species shows considerable variation in growth rate and maximum size among populations. Lohavanijaya (1965) used the average of the length and width of the test as a diameter measure to account for variations in the length/width ratio of *E. parma.* He showed a nearly linear relationship between diameter and the number of pore-pairs in the petals.

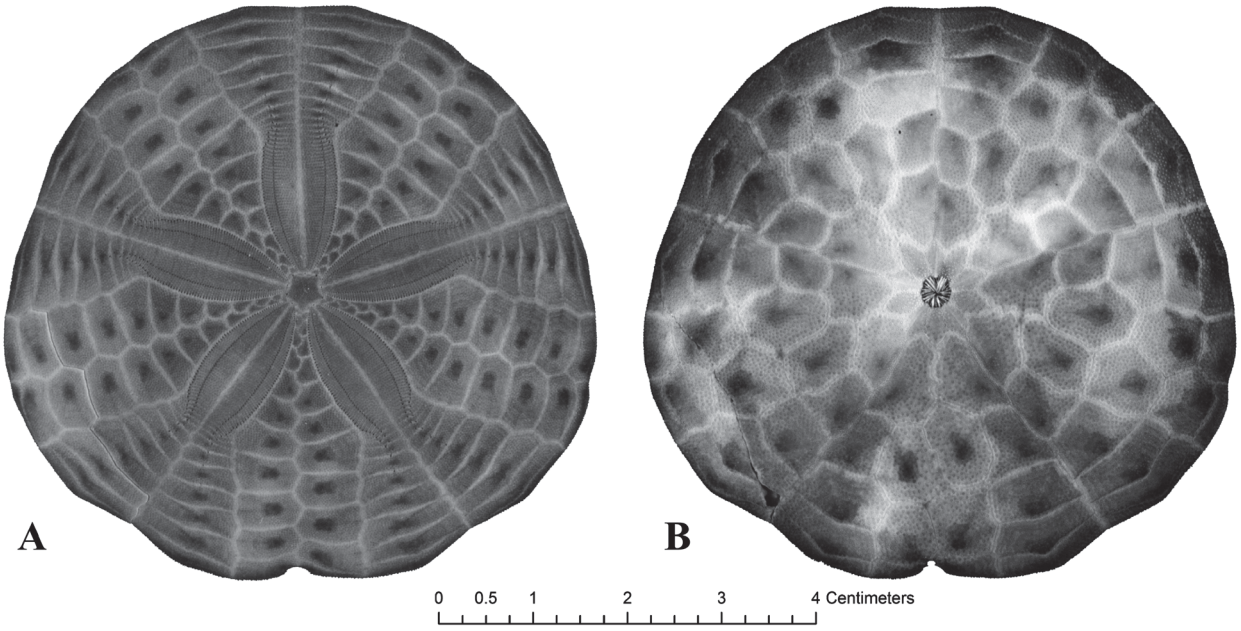

FIGURE 3. *Echinarachnius parma* stained with FD&C Blue to show growth bands. Dorsal viewpoint. A. Aboral. B. Oral (mirrored).

Based on oral plate growth banding there is a linear relationship between the number of growth bands and the total length (estimated from the cumulative areas of the plates for corresponding growth bands) of the test. Therefore, for this ontogenetic study of a single population, length is used as a proxy for age. The spawning period for *E. parma* (Cocanour & Allen 1967) is November-December, implying that the smallest specimens in the study group (2 mm length) were less than 10 months old when collected. The largest specimens (> 70mm length) have growth banding that indicates ages of at least 7 years.

Plate homology. The question of plate homology across an ontogenetic series is not trivial. Traditionally, plate homology on the oral surface of scutelliform echinoids has been based on plate cohort number (although the terminology has been the plate count with reference to the basicoronal set of plates). This is justified by the relatively constant number of plates on the oral surface. There is, however, some variation in the total number of oral plates as a result of variation in the cohort number of plates along the margin.

Cohort number can be continued across the margin and onto the aboral surface, but the disparity in plate addition and growth rates between the ambulacral and interambulacral columns alters the relative position of the plates during ontogeny (Figure 4). A critical concern is how to continue cohort number around the margin. A direct count of plates is not always possible because it is nearly impossible to differentiate the plate sutures on the margin without destroying the specimen. Some of the oral plates are derived from the rudiment (Gordon 1929) but can still be unequivocally assigned to a cohort. Plate homology on the aboral surface is determined by continuous counting of cohorts along columns and around the margin using the ¼ rule described earlier.

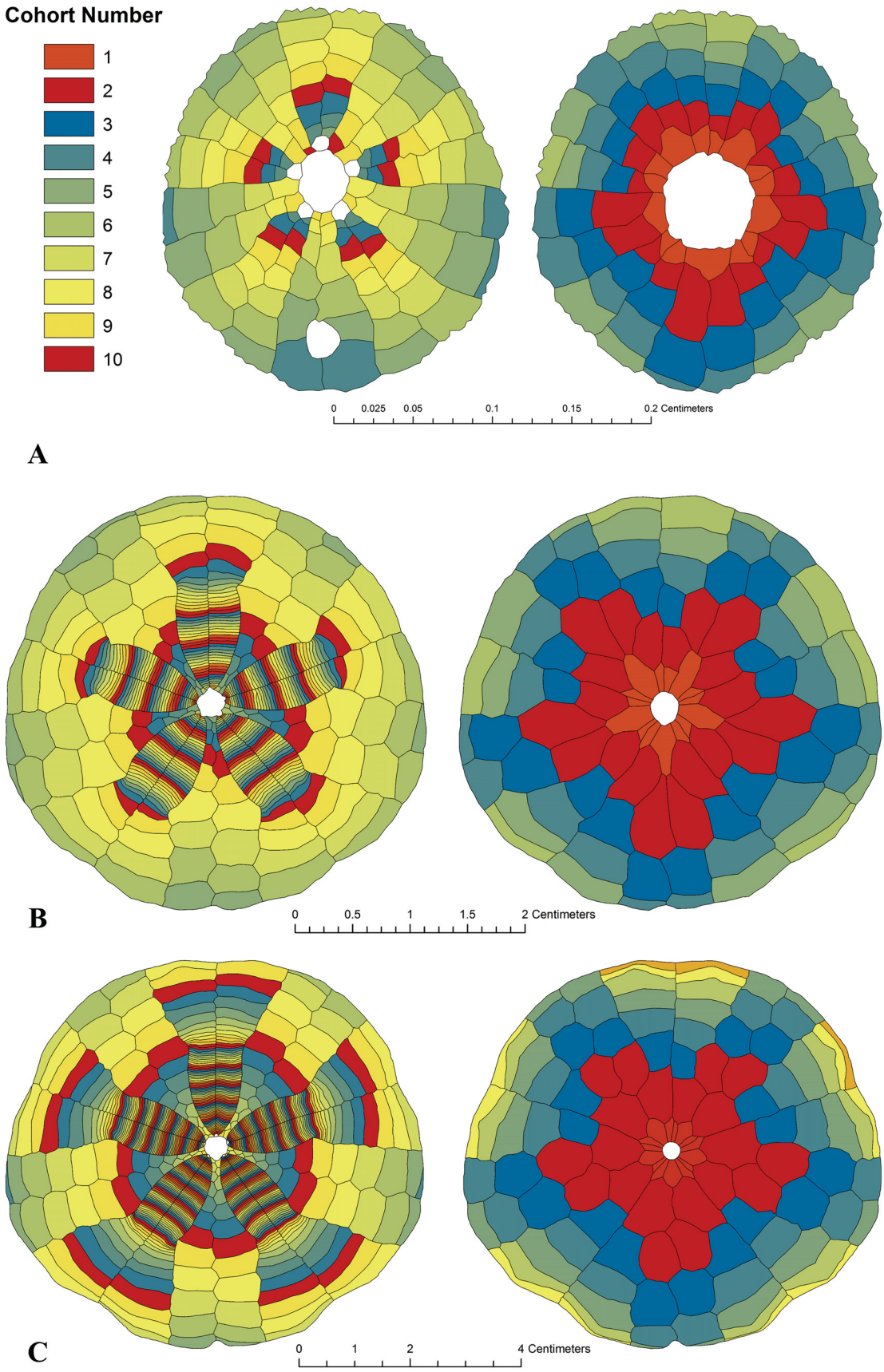

FIGURE 4. Plate diagrams colored by cohort number. Scale restricted to the first 10 cohorts, but color patterns are consistent for later cohorts. Dorsal viewpoint (oral surface is mirrored). A. Juvenile specimen, length 2.45mm B. Immature specimen, length 36mm. C. Adult specimen, length 70mm.

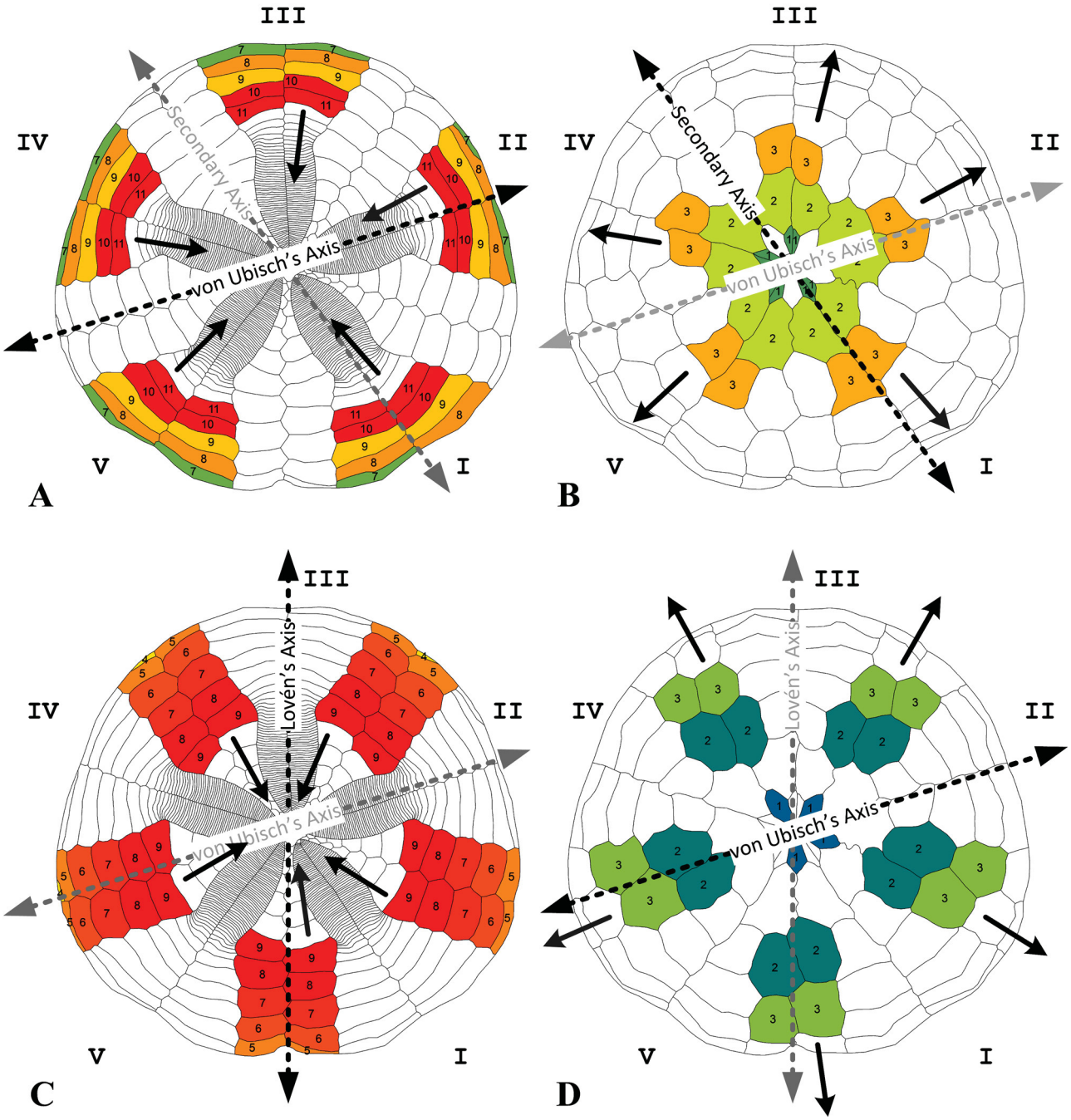

FIGURE 5. Symmetries based on leading/trailing series of plate cohorts. Dorsal viewpoint (oral surface is mirrored). Arrows represent leading columns. A. Aboral ambulacral plates, showing symmetry aligned with von Ubisch's axis. B. Oral ambulacral plates, showing symmetry aligned with secondary "Echinid" axis. C. Aboral interambulacral plates, showing symmetry aligned with Lovén's axis. D. Oral interambulacral plates, showing symmetry aligned with von Ubisch's axis.

The patterning of the plates supports the reasoning that the marginal plating is formed by splitting. In each column (ambulacral and interambulacral) the alternating pattern ("zigzag sutures") means that one plate is leading and the other trailing. Using an ordering convention based on a set of vectors originating in the peristome and extending outward along each plate half-column (20 vectors in all), 10 of these are considered leading if they reach a plate with a given cohort before the vector in the other half-column, which is considered trailing. In the ambulacral columns this convention is such that the trailing columns in the ambulacra are always in the a-a-b-a-b order following Lovén's Rule (Lovén 1874; David *et al.* 1995), and the interambulacral trailing columns in the corresponding b-a-b-a-a order. This ordering must continue onto the aboral surface, regardless of how many

marginal plates there really are, and defines three symmetries (Figure 5). Two symmetries apply to interambulacral plates with one symmetry plane running through the apical system and periproct, and another through the centerline of ambulacrum II and interambulacrum 4. The former axis is identical with Lovén's axis (Lovén 1874), the latter with von Ubisch's primordial axis (Ubisch 1913; Ubisch 1927; Hyman 1955: fig. 219). The two corresponding ambulacral symmetry planes are rotated clockwise 72°, such that the equivalent of Lovén's axis coincides with von Ubisch's axis and the equivalent of the latter passes through the centerline of ambulacrum I and interambulacrum 3, the "Echinid" plane of Gordon (1929: fig. 17). These symmetries would be broken if the marginal plates were from independent cohorts. Only von Ubisch's axis preserves overall symmetry.

Plate growth

An understanding of the overall growth of an echinoid is not possible without first understanding the growth of an individual plate. Zachos (2009) described echinoid plate growth using the linear Bertalanffy (1938) model, based on growth line studies by Deutler (1926). This model is a good match for individual plate growth in regular echinoids, in which the columns are regular and the shape of the corona is broadly domal.

In the case of *E. parma*, the columns are irregular and the discoid shape and development of petals result in strong geometric constraints on plate number and shape. There are two independent but complementary methods for examination of plate growth. The first method is to use the growth bands of individual plates as a record of growth, and the second is to compare homologous plates across an ontogenetic series of individuals as a record of growth. Plate homology is evident on the oral surface, where each plate can be readily assigned by column and position referenced to the basicoronal set of plates surrounding the peristome. This relative position represents the cohort of any given plate. Plates are added to the corona from the edge of the apical system generally in cohorts of 10 (with minor variation and errors in natural plate addition), independently for ambulacral and interambulacral column sets (Zachos 2009; Zachos & Sprinkle 2011).

It is apparent, using either method, that individual plate growth does not follow a strict Bertalanffy model. The best fitted models are logistic (Feller 1940), i.e., with exponential growth in the early stage and exponential decline of growth at a late stage. This is the pattern seen in the diametrical growth of the sea urchin *Strongylocentrotus droebachiensis* (Johnson *et al.* 2013), which has been modeled with various functions (Rogers-Bennett *et al.* 2003). The application of the Verhulst-Pearl logistic process (Pianka 2000), typically used in models of population growth, to model plate growth can be justified as a special case of the Bertalanffy model, in which growth is promoted by a nutritive resource which diffuses outwards from a plate center and is thus regulated by plate size. This plate growth model in differential form is:

$$\frac{dS}{dt} = rS\left(\frac{K-S}{K}\right)$$

where S is the size of the plate, K is the maximum size, and r is the maximum rate of change.

The logistic equation can be solved for the size S at time t by:

$$S(t) = \frac{K}{1 + e^{-r(t-t_o)}}$$

where t_o is the time taken for the plate to reach half its maximum size (which represents the inflection point of the logistic curve). In this case, test length is used as a proxy for time, and thus t_o represents the test length at which the plate reaches half its maximum size.

Separate logistic equations were fit to the ontogenetic series of homologous plate areas using the nonlinear least squares regression method (Ebert 2013) in MATLAB®. The result is a complete set of logistic coefficients K, r, and t_o for each plate in the corona. The majority of the plates clearly show sigmoidal growth curves (Figure 6A, B). However, determination of the exact parameters defining the logistic equation for each plate is confounded in part by uncertainty concerning the actual age of any given echinoid at the time of measurement as well as minor variations in homologous plate locations, particularly along the margins. These uncertainties are compounded by the exponential nature of the growth curves, resulting in a noisy pattern when the parameters are plotted against presumptive plate age (cohort number).

Although most of the plates can be fit with a logistic model, for a significant number the asymptote of the logistic curve is large, and the curves approximate a quadratic within the normal length range. If the quadratic term is removed by plotting the plate areas against the total area of the test rather than the test length, a simple linear relationship becomes apparent (Figure 6C, D). This relationship is more robust with regard to uncertainties in measurement or plate homology than the logistic model. The relationship represents the proportion of test growth attributable to each plate, can be represented by a single parameter (slope) if the intercept is constrained to 0 (using the singular value decomposition method to fit the data), and is more readily understood in terms of growth domains than the logistic model.

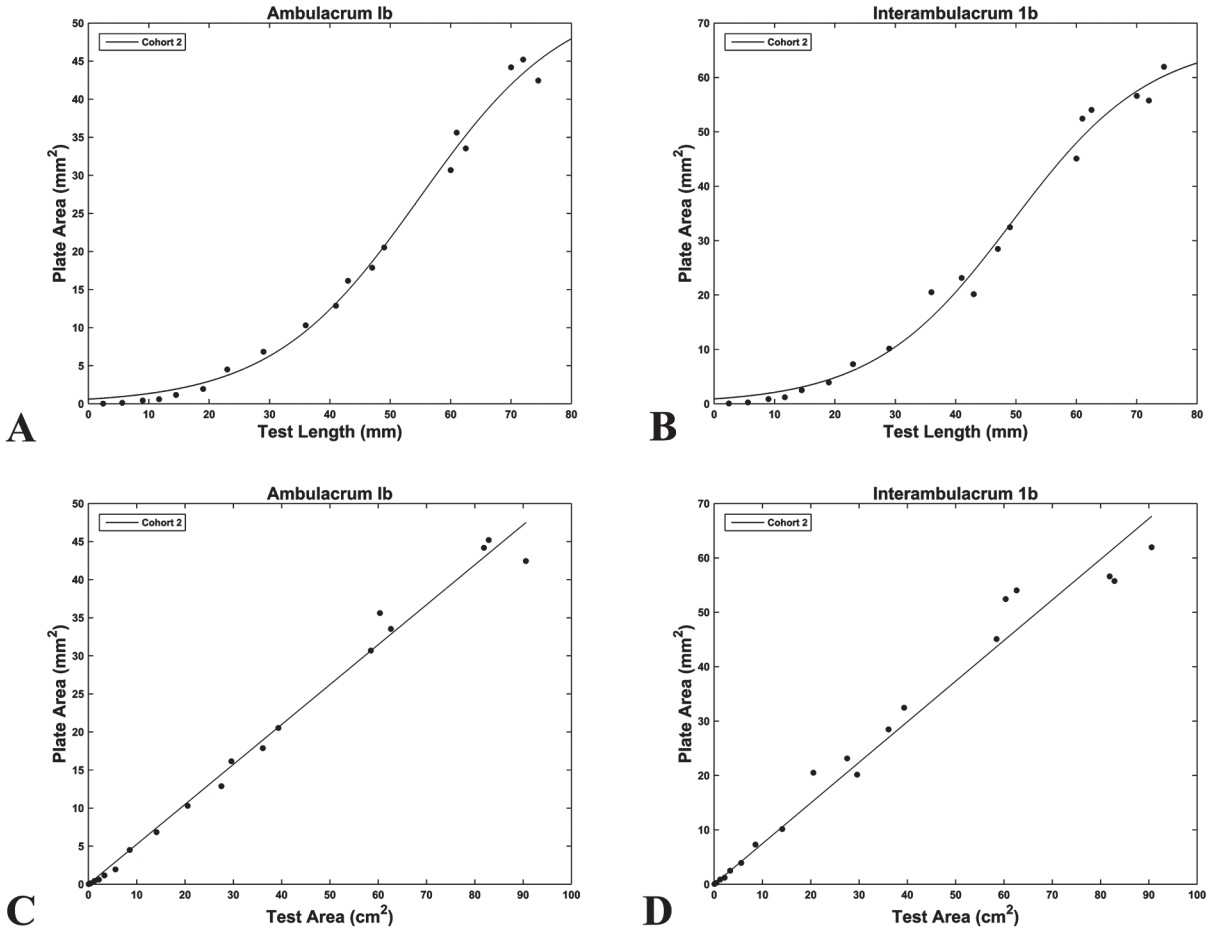

FIGURE 6. Representative growth curves for individual plates. Logistic function for plate area (mm^2) vs. test length (mm) fitted to data. A. Ambulacrum Ib, cohort 2. B. Interambulacrum 1b, cohort 2. Linear function for plate area (mm^2) vs. total test area (cm^2) fitted to data. C. Ambulacrum Ib, cohort 2. D. Interambulacrum 1b, cohort 2.

Plate domains

Echinoids are characterized by an invariant process of plate addition. At metamorphosis (or the equivalent point for direct-developing echinoids), the very young echinoid (or imago) skeleton is composed of the apical system of genital, ocular, and periproctal plates and a variable number of coronal plates. During ontogeny, new plates are added to the corona from points distributed around the apical system, in conformance with the Ocular Plate Rule (Mooi & David 1997), valid for all modern echinoids. Plates are added in complete cycles around the apical system in cohorts such that the plates form domains representing specific periods of addition and growth (Zachos 2009). *Echinarachnius parma* demonstrates considerable variance in the number of plates in the imago at metamorphosis, ranging from 38 to 53 in one set of examples (Gordon 1929). This will invariably include 10 ambulacral and 5 interambulacral basicoronal plates around the peristome along with one or two cohorts of additional coronal plates. The periproct is initially located within the apical system at this stage, but becomes associated with the next or

fourth cohort (the third post-basicoronal cohort), and with the addition of new plates it moves progressively farther from the apical system. The imago is essentially spherical in shape at this stage, but with the addition of between two or three more plate cohorts, the corona undergoes flattening with the creation of fixed margin plates and 'freezing' of the number of oral plates. This abrupt morphologic event will be termed 'fold-over'.

Fold-over marks a critical benchmark in ontogenetic development. The early-stage ambulacral plates are equivalent in size with the interambulacral plates, which indicates that the rate of plate addition was the same in all plate columns. At fold-over, ambulacral plate addition doubles in rate relative to interambulacral plate addition, resulting in a 2:1 ambulacral to interambulacral (A:I) plate ratio (see Figure 4A). This change in addition rate creates a significant disparity in plate sizes between the columns, and creates two distinct plate domains: (1) plates in the equal-sized domain outside (distal from) the petalodium, which will be termed 'early'; (2) plates inside the petalodium, which will be termed 'juvenile'. The term petalodium is used here in the sense of Nebelsick & Kowalewski (1999) to include both ambulacral and interambulacral plates that lie within the area formed by the tips of the petals. Although this differs from the original definition of petalodium (Lang 1896) as synonymous with the petals themselves, recent usage (e.g. Grun *et al.* 2014; Sievers & Nebelsick 2014) favors the more expansive definition. Another aspect of fold-over is that at this point the oral and aboral plates begin to form skeletal connections (buttresses and pillars), with the effect that the growth of individual aboral plates in the early domain is constrained by the growth of the corresponding oral plates.

Following fold-over, interambulacral plate addition slows relative to ambulacral plate addition such that the A:I ratio increases to around 6:1 (Figure 4B). This is the juvenile period of growth, and the majority of the remaining interambulacral plates are added during this period of growth, creating the juvenile domain of interambulacral plates.

At the end of the juvenile period, the genital pores penetrate the last interambulacral plates to be added, slowing or effectively ending the addition of new interambulacral plates. However, new ambulacral plates continue to be added throughout the adult stage of growth and are accommodated by the growth of the interambulacral plates and translocation of plates along the adradiad sutures between the two columns, settling on an A:I ratio of about 10:1 (Figure 4C). Because of translocation, it is difficult or impossible to distinguish juvenile from adult stage ambulacral plates, but one aspect of adult stage ambulacral plate addition is the formation of impacted plates at the tips of the petals. Although this impaction leads to plate occlusion in some scutelliforms, it does not in *E. parma*. The degree of plate impaction is a measure of the degree to which ambulacral plate addition outpaced interambulacral plate growth in the latest stage of adult growth.

There are, therefore, four major stages of plate addition that can be distinguished in separate domains of plate cohorts in the corona of *E. parma*: (1) development of the imago skeleton just prior to metamorphosis (cohorts 1 & 2); (2) early growth associated with expansion of the corona and relative displacement of the periproct away from the apical system by addition of intervening plates ending with fold-over (ambulacral cohorts 3-5, interambulacral cohorts 3 & 4); (3) juvenile growth with formation of the petals and addition of juvenile interambulacral plates ending with the extrusion of the genital pores (up to about cohort 10 in all columns); and (4) adult growth with a limited number of new interambulacral plates but continued addition of ambulacral plates.

Growth domains

The progression of growth stages is preserved in distinct groups of plates. These groups are termed, in accordance with the respective growth stages, (1) rudimental plates, (2) imaginal plates, (3) juvenile plates, and (4) adult plates. The rudimental plates, so carefully described by Gordon (1929), include the primordial genital and ocular plates (derived at least in part directly from the larval spicules) and a small set of coronal plates varying somewhat in number, which lack any suturing. The imaginal plates are those plates present after metamorphosis and settlement of the larva, at which point the existing plates are weakly sutured into a complete mosaic. The most important characteristic of this stage of development is that the periproct (covered by a single periproctal plate) is in direct contact with the apical system. The juvenile plates incorporate those cohorts of plates that are added to the corona adapically of the periproct following recruitment, but before any petaloid ambulacral plates are added. The final adult plates are added to the corona beginning with the appearance of the first petaloid plates. Differentiation of plating on the aboral and oral surfaces of an echinoid (as divided approximately by being above or below the

ambitus, respectively) is characteristic of irregular echinoids (Smith 2005), and is most extreme in the sand dollars, in which the ambitus forms a distinct boundary. Two important consequences of this are (1) the oral surface of *E. parma* includes only rudimental and imaginal plates, and (2) subsequent growth of the oral plates is linked to juvenile and adult growth of aboral plates.

Relationship to traditional systems

Traditionally, several plate domains in the sand dollar (and other) echinoids have been specially delineated for purposes of morphologic description. The set of plates surrounding the peristome is traditionally termed the basicoronal circlet, and here is referenced as cohort 1. These plates are the first to appear in the rudiment and the relative size of the ambulacral plates in the individual columns form the basis of the Lovén Rule of symmetry – in every sense they can be considered the primordial coronal plates. The cohorts of plates surrounding the basicoronal circlet are grouped into post-basicoronal plates, and numbered in accordance with the respective cohort set (i.e., first post-basicoronal plates, second, etc.). However, in the specific case of *E. parma,* this system ignores the fact that one or two of the post-basicoronal plates are also formed in the rudiment. Some significance has been associated with separation of the first post-basicoronal interambulacral plates from the basicoronal plates (Durham 1955; Lohavanijaya & Swan 1965). Terminology in this study references these plates in cohort order, i.e., the first post-basicoronal plates are cohort 2, etc.

Moore & Ellers (1993) delineated a peripheral ring of plates associated with a belt of dense calcite formed by the internal pillars and buttresses lining the oral and aboral plates. Regardless of the functional utility of these buttresses, their location and development define a specific region of the test. The peripheral ring lies outside of the region defined (on the aboral side) by the extent of the petaloid ambulacra, or petalodium as used here. Structurally, the petalodium region lacks the buttressing characteristic of the peripheral ring.

Plate addition

Plates are added to the corona throughout the life of the animal. Using length as a proxy for age, the rate of plate addition decreases in a systematic fashion as the animal ages (Figure 7). The variation in the number of plate cohorts associated with any particular plate column appears to be random. The number of plates in the ambulacral vs. the interambulacral columns is nearly the same in the youngest individuals, but the total numbers increasingly diverge with growth. The maximum number of 16 or 17 interambulacral plate cohorts is reached by a length of about 60mm. The number of ambulacral cohorts, though declining in addition rate, increases throughout the life of the animal. The coefficients of the quadratic fitting equations (Figure 7) for the number of plate cohorts y as a function of test length x (in centimeters) are:

Ambulacra $y = -0.6653x^2 + 14.197x + 11.499$

Interambulacra $y = -0.091697x^2 + 1.477x + 10.431$

Allometric growth

Plate growth patterns between ambulacral and interambulacral columns in *E. parma* are distinctly different, and thus define two separate growth domains. In addition, the limitation that the oral surface is composed of only rudimental and imaginal plates while the aboral coronal surface is composed of only juvenile and adult plates further divides the test into two additional distinct growth domains. In the former case the two domains are correlated laterally, whereas in the latter case the two domains are correlated vertically. The allometric growth patterns might also be expected to show similar correlations.

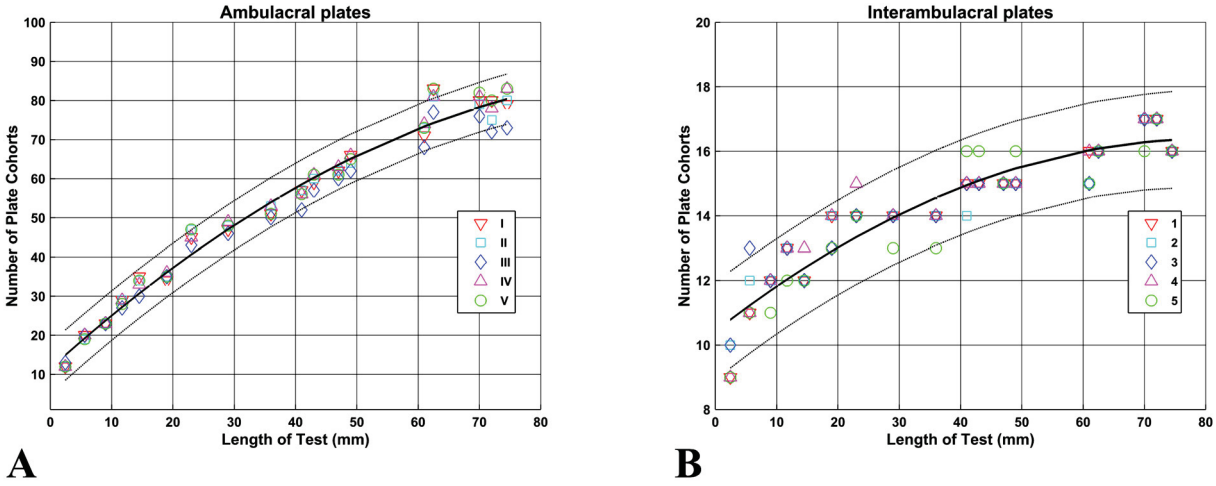

FIGURE 7. Number of plate cohorts as a function of test length. A. Ambulacral plates. B. Interambulacral plates. Solid line is a second-order (quadratic) least-squares fit to the data, with 95% confidence interval delineated with dotted lines.

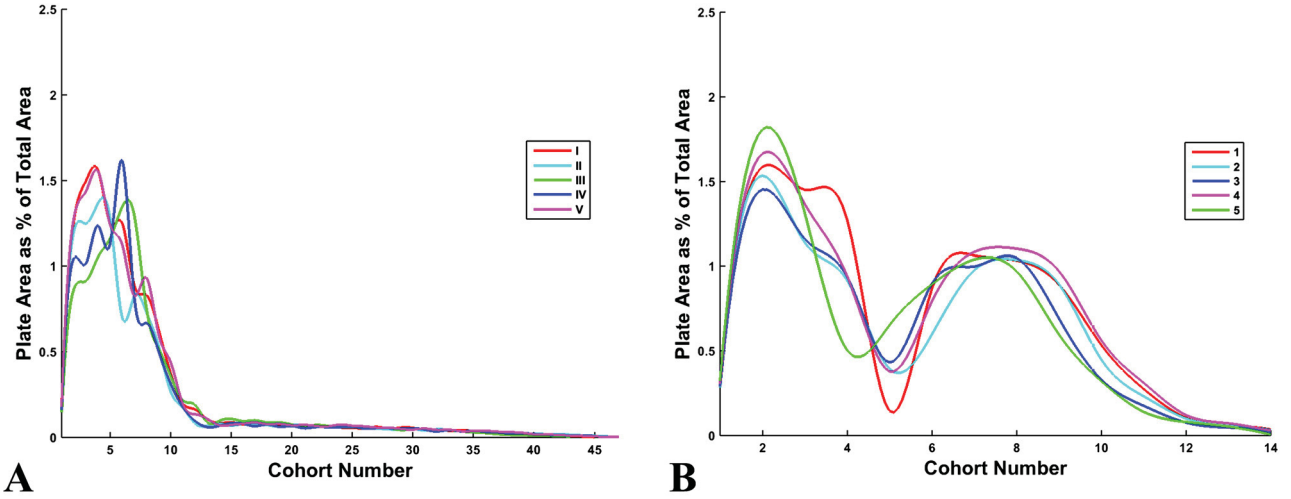

FIGURE 8. Plate area as a percentage of total test area by cohort number. Data points interpolated by cubic splines. A. Ambulacral plates for specimen 23mm length. B. Corresponding interambulacral plates for same specimen. Colors are associated with individual plate columns, combining both half columns. Roman numerals for ambulacra, Arabic numerals for interambulacra.

If plate area, as the dependent variable, is plotted against cohort number for each of the twenty columns measured, the resulting graph represents the range of plate sizes as a function of their relative age. If plate areas are normalized by total test area, resulting in proportional area measures, the graphs between different specimens of different absolute ages can be compared directly. The set of 20 graphs for each specimen can be divided into two sets of 10 columns (representing the ambulacral and interambulacral columns) and these sets averaged across half columns and smoothed, resulting in a graph for each of the 5 full columns of the two column domains (Figure 8).

The individual graphs can themselves be graphed along another axis representing test length (Figure 9A) and then used to generate a set of continuous surfaces representing the size of plates by cohort by length (Figure 9B). These surfaces can be summed to generate a single surface incorporating all of the ambulacral or interambulacral plates across the entire ontogenetic series (Figure 9C).

The marginal plates, because of their restricted size, form a local minimum in the surface separating the oral plates (low cohort numbers) from the aboral plates (high cohort numbers). The relationships are more readily interpreted by contour maps of the surfaces (Figure 10). The largest interambulacral plates are those of the 2nd and 3rd cohorts orally, and the 7th and 8th cohorts aborally. The largest ambulacral plates are generally the 4th and 5th orally, and also the 8th and 9th aborally, dropping rapidly in the plates of the petals.

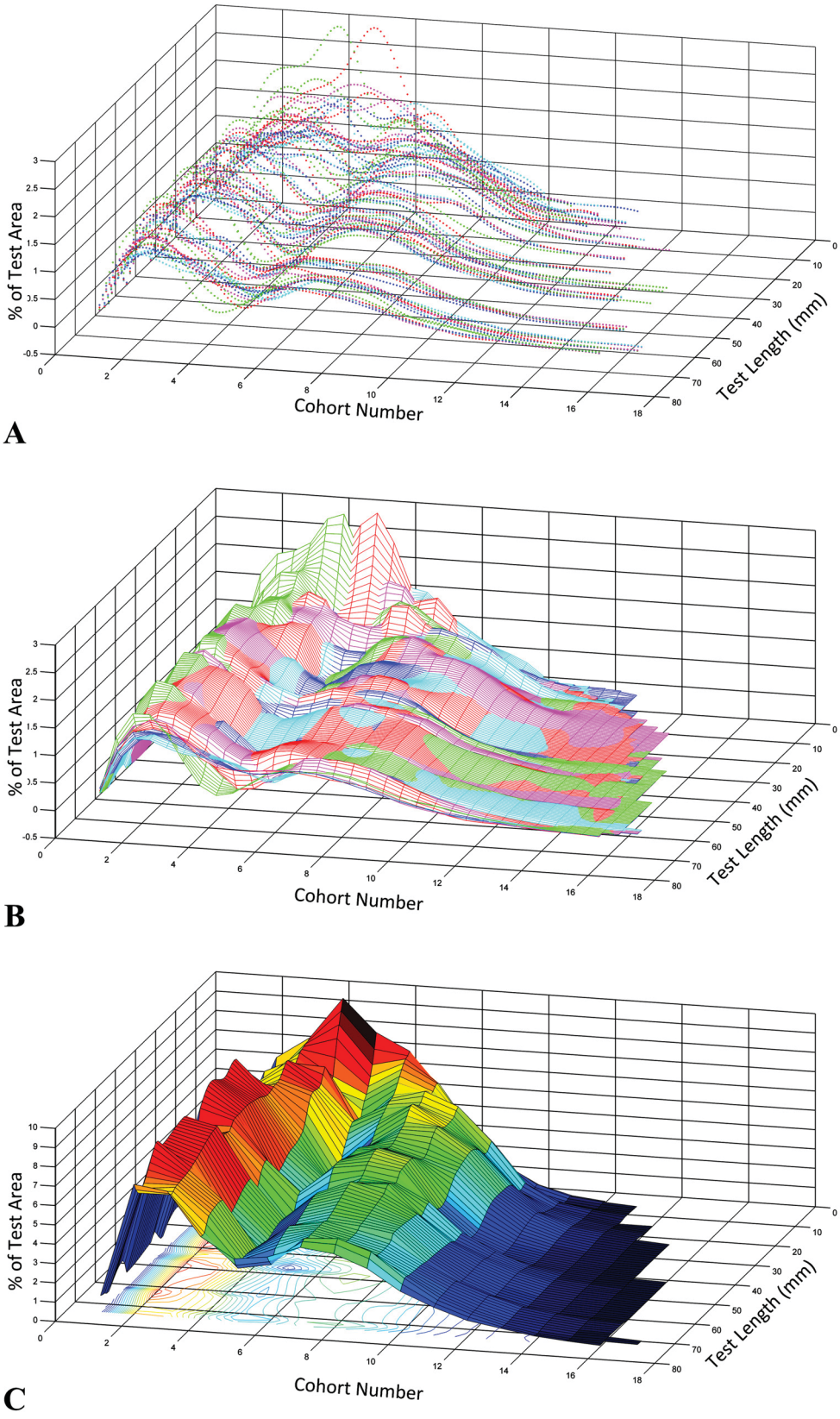

FIGURE 9. Composite of plate area as a percentage of total test area by cohort number by test length for interambulacral plates. Test length increases towards viewer. A. Individual plate area functions. Colors are associated with individual plate columns, combining both half columns. B. Surface interpolations of individual plate area functions. C. Surface interpolation of the sum of plate area functions. Contours are projected onto the cohort number vs. test length base plane.

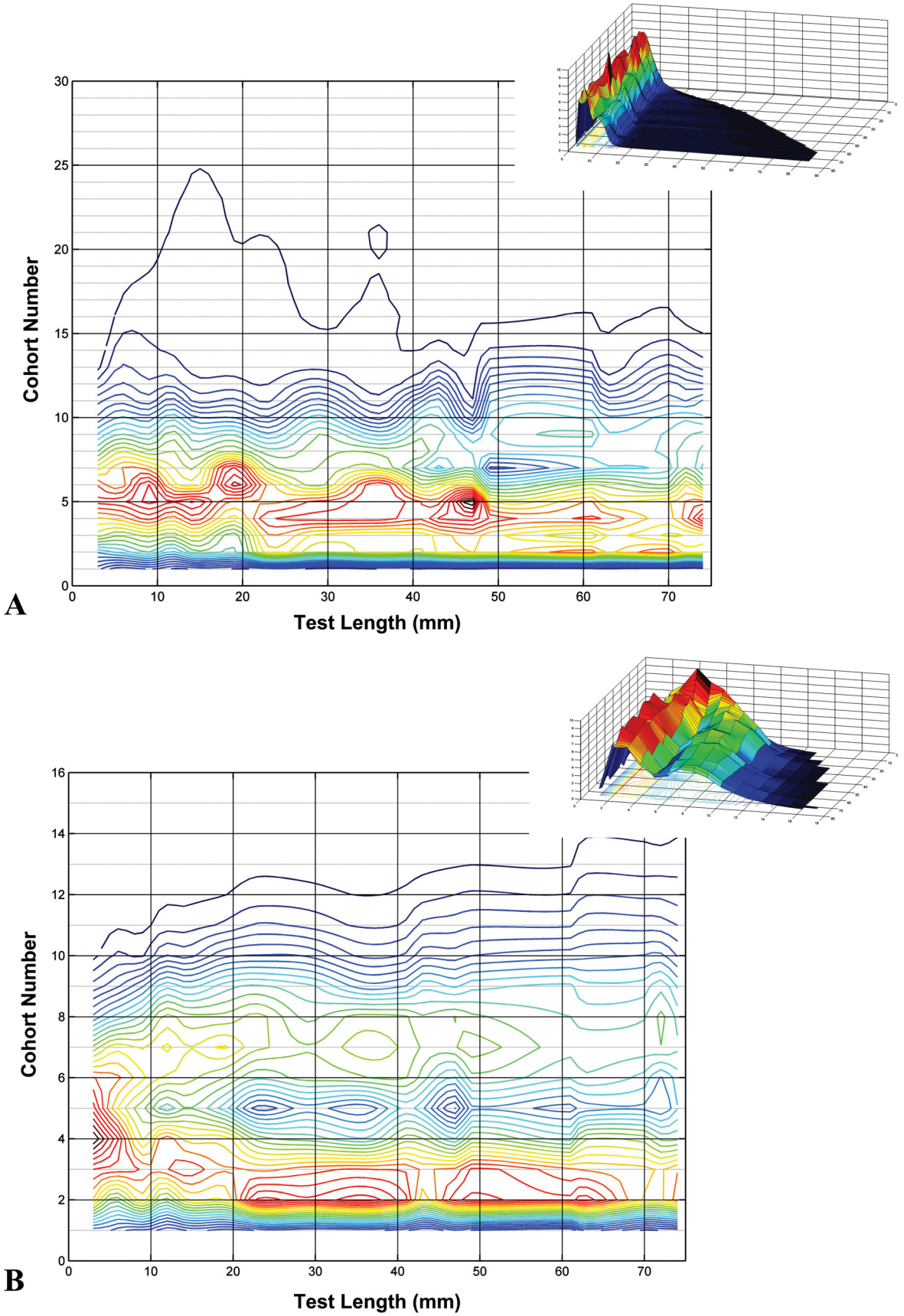

FIGURE 10. Contour maps of plate area surfaces projected onto the cohort number vs. test length plane. Contour interval is 0.25%. Insets show corresponding 3D surfaces. A. Ambulacral plates. B. Interambulacral plates.

Another way to visualize the allometry in plate growth is to map the rate of change in plate area on a representative plate template. The slopes derived from the linear growth curves (Figure 6C, D) which are based on the normalized plate areas can be used to represent relative growth rate. Using one of the larger specimens as a mapping template the centers of each plate can be assigned the corresponding slope (growth rate) value and the points gridded and contoured (Figure 11). Any plate template can be used, and the results are similar in every case (because the point locations are defined by column and cohort number, both of which are nearly constant positionally for adults regardless of the exact specimen age). Slope data are given in Tables 1 and 2 for interambulacral and ambulacral plates, respectively.

TABLE 1. Slopes for interambulacral plates up to cohort 16. Slope units are plate area in mm^2 over total test surface area in cm^2.

Plate Id	Slope	Plate Id	Slope	Plate Id	Slope	Plate Id	Slope	Plate Id	Slope
1a01	0.183758	-	-	2a01	0.176035	-	-	3a01	0.227144
1a02	0.686176	1b02	0.746700	2a02	0.679153	2b02	0.547619	3a02	0.554412
1a03	0.758881	1b03	0.682213	2a03	0.562498	2b03	0.523185	3a03	0.530910
1a04	0.577290	1b04	0.416782	2a04	0.474918	2b04	0.482110	3a04	0.509358
1a05	0.327477	1b05	0.259319	2a05	0.294939	2b05	0.391040	3a05	0.343329
1a06	0.378524	1b06	0.416479	2a06	0.369544	2b06	0.281223	3a06	0.322377
1a07	0.468175	1b07	0.430437	2a07	0.409385	2b07	0.401921	3a07	0.423781
1a08	0.442705	1b08	0.393991	2a08	0.416356	2b08	0.411915	3a08	0.400421
1a09	0.389496	1b09	0.309176	2a09	0.317302	2b09	0.358455	3a09	0.366903
1a10	0.267049	1b10	0.199143	2a10	0.200526	2b10	0.256441	3a10	0.246122
1a11	0.164712	1b11	0.118651	2a11	0.131342	2b11	0.158052	3a11	0.151832
1a12	0.093109	1b12	0.062687	2a12	0.076423	2b12	0.105401	3a12	0.098706
1a13	0.047809	1b13	0.042330	2a13	0.045353	2b13	0.061785	3a13	0.054299
1a14	0.025059	1b14	0.022044	2a14	0.024110	2b14	0.033854	3a14	0.026842
1a15	0.013884	1b15	0.009659	2a15	0.010286	2b15	0.013930	3a15	0.013801
1a16	0.006546	1b16	0.004146	2a16	0.005711	2b16	0.004547	3a16	0.006132

Plate Id	Slope	Plate Id	Slope	Plate Id	Slope	Plate Id	Slope	Plate Id	Slope
-	-	4a01	0.175405	-	-	5a01	0.198122	-	-
3b02	0.707501	4a02	0.759396	4b02	0.685849	5a02	0.769798	5b02	0.754633
3b03	0.606986	4a03	0.655642	4b03	0.765215	5a03	0.630235	5b03	0.717676
3b04	0.458378	4a04	0.424164	4b04	0.557845	5a04	0.206175	5b04	0.351791
3b05	0.243246	4a05	0.271778	4b05	0.353868	5a05	0.203497	5b05	0.099507
3b06	0.386173	4a06	0.398140	4b06	0.364374	5a06	0.381853	5b06	0.306327
3b07	0.405891	4a07	0.436714	4b07	0.464437	5a07	0.437816	5b07	0.426023
3b08	0.391112	4a08	0.393286	4b08	0.443796	5a08	0.406073	5b08	0.429076
3b09	0.297440	4a09	0.320321	4b09	0.389422	5a09	0.313426	5b09	0.380197
3b10	0.192035	4a10	0.194770	4b10	0.262244	5a10	0.194670	5b10	0.255781
3b11	0.118954	4a11	0.115856	4b11	0.166411	5a11	0.123061	5b11	0.172899
3b12	0.071595	4a12	0.065848	4b12	0.097826	5a12	0.071909	5b12	0.102951
3b13	0.036172	4a13	0.040612	4b13	0.052158	5a13	0.039454	5b13	0.056488
3b14	0.018653	4a14	0.023261	4b14	0.026468	5a14	0.022565	5b14	0.032718
3b15	0.009453	4a15	0.010792	4b15	0.010514	5a15	0.014261	5b15	0.016309
3b16	0.002962	4a16	0.004793	4b16	0.007374	5a16	0.005937	5b16	0.011187

TABLE 2. Slopes for ambulacral plates up to cohort 83. Slope units are plate area in mm^2 over total test surface area in cm^2.

Plate ID	Slope	Plate ID	Slope	Plate ID	Slope	Plate ID	Slope	Plate ID	Slope
Ia01	0.058288	Ib01	0.038082	IIa01	0.058396	IIb01	0.000427	IIIa01	0.041946
Ia02	0.661363	Ib02	0.524292	IIa02	0.701956	IIb02	0.005122	IIIa02	0.405974
Ia03	0.650911	Ib03	0.591300	IIa03	0.497306	IIb03	0.004017	IIIa03	0.378672
Ia04	0.761945	Ib04	0.774092	IIa04	0.646012	IIb04	0.005629	IIIa04	0.533800
Ia05	0.587854	Ib05	0.657508	IIa05	0.625851	IIb05	0.006508	IIIa05	0.560139
Ia06	0.306268	Ib06	0.510653	IIa06	0.486357	IIb06	0.005542	IIIa06	0.532847
Ia07	0.315874	Ib07	0.261483	IIa07	0.384857	IIb07	0.003451	IIIa07	0.396678
Ia08	0.395963	Ib08	0.416641	IIa08	0.376871	IIb08	0.003649	IIIa08	0.267275
Ia09	0.379804	Ib09	0.405049	IIa09	0.366186	IIb09	0.003984	IIIa09	0.362919
Ia10	0.293814	Ib10	0.337242	IIa10	0.281012	IIb10	0.003191	IIIa10	0.357265
Ia11	0.217996	Ib11	0.283500	IIa11	0.217748	IIb11	0.002513	IIIa11	0.291753
Ia12	0.151913	Ib12	0.195933	IIa12	0.141210	IIb12	0.001796	IIIa12	0.239494
Ia13	0.080805	Ib13	0.118699	IIa13	0.073962	IIb13	0.001055	IIIa13	0.141678
Ia14	0.052223	Ib14	0.074401	IIa14	0.043712	IIb14	0.000569	IIIa14	0.093994
Ia15	0.032428	Ib15	0.044750	IIa15	0.031199	IIb15	0.000381	IIIa15	0.055721
Ia16	0.023950	Ib16	0.031380	IIa16	0.026271	IIb16	0.000290	IIIa16	0.042164
Ia17	0.024025	Ib17	0.025543	IIa17	0.024400	IIb17	0.000250	IIIa17	0.032066
Ia18	0.022359	Ib18	0.022903	IIa18	0.021098	IIb18	0.000223	IIIa18	0.029808
Ia19	0.020492	Ib19	0.022932	IIa19	0.020645	IIb19	0.000210	IIIa19	0.028238
Ia20	0.019856	Ib20	0.019738	IIa20	0.019259	IIb20	0.000200	IIIa20	0.026205
Ia21	0.020426	Ib21	0.019586	IIa21	0.019434	IIb21	0.000196	IIIa21	0.024373
Ia22	0.020211	Ib22	0.021352	IIa22	0.016989	IIb22	0.000195	IIIa22	0.024760
Ia23	0.019123	Ib23	0.019972	IIa23	0.019068	IIb23	0.000180	IIIa23	0.022048
Ia24	0.017972	Ib24	0.019087	IIa24	0.017842	IIb24	0.000175	IIIa24	0.022851
Ia25	0.017227	Ib25	0.020001	IIa25	0.018575	IIb25	0.000187	IIIa25	0.021688
Ia26	0.018864	Ib26	0.018420	IIa26	0.017730	IIb26	0.000188	IIIa26	0.020097
Ia27	0.017792	Ib27	0.017851	IIa27	0.016269	IIb27	0.000171	IIIa27	0.021601
Ia28	0.018966	Ib28	0.018253	IIa28	0.016428	IIb28	0.000168	IIIa28	0.021077
Ia29	0.018484	Ib29	0.017682	IIa29	0.017409	IIb29	0.000175	IIIa29	0.020225
Ia30	0.018795	Ib30	0.016063	IIa30	0.017350	IIb30	0.000165	IIIa30	0.019792
Ia31	0.019460	Ib31	0.019665	IIa31	0.017394	IIb31	0.000164	IIIa31	0.018507
Ia32	0.018170	Ib32	0.017491	IIa32	0.017042	IIb32	0.000172	IIIa32	0.019396
Ia33	0.017701	Ib33	0.017270	IIa33	0.016791	IIb33	0.000161	IIIa33	0.020398
Ia34	0.018505	Ib34	0.017458	IIa34	0.016225	IIb34	0.000170	IIIa34	0.018187
Ia35	0.017638	Ib35	0.018104	IIa35	0.016958	IIb35	0.000165	IIIa35	0.019667
Ia36	0.017442	Ib36	0.016655	IIa36	0.016428	IIb36	0.000165	IIIa36	0.018198
Ia37	0.017143	Ib37	0.016323	IIa37	0.016974	IIb37	0.000160	IIIa37	0.018011
Ia38	0.018090	Ib38	0.016202	IIa38	0.016594	IIb38	0.000153	IIIa38	0.017668
Ia39	0.015312	Ib39	0.017348	IIa39	0.015724	IIb39	0.000159	IIIa39	0.017019
Ia40	0.016442	Ib40	0.016969	IIa40	0.015805	IIb40	0.000155	IIIa40	0.018030
Ia41	0.017133	Ib41	0.016230	IIa41	0.015796	IIb41	0.000157	IIIa41	0.016500

.....continued on the next page

TABLE 2. (Continued)

Plate ID	Slope	Plate ID	Slope	Plate ID	Slope	Plate ID	Slope	Plate ID	Slope
Ia42	0.016089	Ib42	0.016334	IIa42	0.015398	IIb42	0.000150	IIIa42	0.016411
Ia43	0.015764	Ib43	0.016714	IIa43	0.014991	IIb43	0.000148	IIIa43	0.016725
Ia44	0.015335	Ib44	0.015382	IIa44	0.014990	IIb44	0.000149	IIIa44	0.015497
Ia45	0.015519	Ib45	0.015252	IIa45	0.014191	IIb45	0.000134	IIIa45	0.014902
Ia46	0.014784	Ib46	0.015018	IIa46	0.01381	IIb46	0.000139	IIIa46	0.015476
Ia47	0.014676	Ib47	0.014931	IIa47	0.013637	IIb47	0.000130	IIIa47	0.015417
Ia48	0.013693	Ib48	0.013832	IIa48	0.013667	IIb48	0.000129	IIIa48	0.014571
Ia49	0.013259	Ib49	0.013598	IIa49	0.012923	IIb49	0.000128	IIIa49	0.013989
Ia50	0.013583	Ib50	0.014008	IIa50	0.012306	IIb50	0.000118	IIIa50	0.014055
Ia51	0.013687	Ib51	0.011701	IIa51	0.012862	IIb51	0.000128	IIIa51	0.012721
Ia52	0.012384	Ib52	0.012847	IIa52	0.011792	IIb52	0.000117	IIIa52	0.012066
Ia53	0.012169	Ib53	0.012562	IIa53	0.012522	IIb53	0.000114	IIIa53	0.012387
Ia54	0.011648	Ib54	0.012121	IIa54	0.011057	IIb54	0.000108	IIIa54	0.011057
Ia55	0.011248	Ib55	0.012358	IIa55	0.010717	IIb55	0.000107	IIIa55	0.010788
Ia56	0.011267	Ib56	0.011408	IIa56	0.010650	IIb56	0.000096	IIIa56	0.010312
Ia57	0.010527	Ib57	0.010682	IIa57	0.010074	IIb57	0.000098	IIIa57	0.009572
Ia58	0.010648	Ib58	0.010797	IIa58	0.009805	IIb58	0.000092	IIIa58	0.009568
Ia59	0.009677	Ib59	0.010009	IIa59	0.008868	IIb59	0.000092	IIIa59	0.007415
Ia60	0.009309	Ib60	0.009190	IIa60	0.008246	IIb60	0.000078	IIIa60	0.008322
Ia61	0.008374	Ib61	0.009518	IIa61	0.007809	IIb61	0.000081	IIIa61	0.007601
Ia62	0.008597	Ib62	0.008556	IIa62	0.007696	IIb62	0.000078	IIIa62	0.006489
Ia63	0.007658	Ib63	0.008023	IIa63	0.007378	IIb63	0.000070	IIIa63	0.006415
Ia64	0.007055	Ib64	0.007851	IIa64	0.006610	IIb64	0.000064	IIIa64	0.005662
Ia65	0.006672	Ib65	0.007712	IIa65	0.006430	IIb65	0.000063	IIIa65	0.005338
Ia66	0.005771	Ib66	0.006984	IIa66	0.005887	IIb66	0.000057	IIIa66	0.004673
Ia67	0.005739	Ib67	0.005983	IIa67	0.005438	IIb67	0.000054	IIIa67	0.004313
Ia68	0.004482	Ib68	0.006256	IIa68	0.005169	IIb68	0.000047	IIIa68	0.003779
Ia69	0.004767	Ib69	0.005406	IIa69	0.004485	IIb69	0.000041	IIIa69	0.003098
Ia70	0.004626	Ib70	0.004657	IIa70	0.004084	IIb70	0.000040	IIIa70	0.002491
Ia71	0.003778	Ib71	0.004384	IIa71	0.003787	IIb71	0.000034	IIIa71	0.001786
Ia72	0.003383	Ib72	0.003358	IIa72	0.003350	IIb72	0.000031	IIIa72	0.001972
Ia73	0.003128	Ib73	0.003017	IIa73	0.002775	IIb73	0.000029	IIIa73	0.001428
Ia74	0.002418	Ib74	0.002822	IIa74	0.002497	IIb74	0.000025	IIIa74	0.000886
Ia75	0.002061	Ib75	0.002607	IIa75	0.002137	IIb75	0.000019	IIIa75	0.000746
Ia76	0.001696	Ib76	0.002124	IIa76	0.001779	IIb76	0.000018	IIIa76	0.000601
Ia77	0.001535	Ib77	0.001892	IIa77	0.001426	IIb77	0.000015	IIIa77	0.000100
Ia78	0.001148	Ib78	0.001465	IIa78	0.001298	IIb78	0.000013	IIIa78	0.000000
Ia79	0.000895	Ib79	0.001011	IIa79	0.000962	IIb79	0.000010	IIIa79	0.000000
Ia80	0.000408	Ib80	0.000621	IIa80	0.000218	IIb80	0.000005	IIIa80	0.000000
Ia81	0.000337	Ib81	0.000304	IIa81	0.000084	IIb81	0.000002	IIIa81	0.000000
Ia82	0.000252	Ib82	0.000302	IIa82	0.000000	IIb82	0.000000	IIIa82	0.000000
Ia83	0.000103	Ib83	0.000152	IIa83	0.000000	IIb83	0.000000	IIIa83	0.000000

.....continued on the next page

TABLE 2. (Continued)

Plate ID	Slope	Plate ID	Slope	Plate ID	Slope	Plate ID	Slope	Plate ID	Slope
IIIb01	0.055142	IVa01	0.059479	IVb01	0.045906	Va01	0.039497	Vb01	0.066881
IIIb02	0.527663	IVa02	0.610453	IVb02	0.575126	Va02	0.509217	Vb02	0.789042
IIIb03	0.468705	IVa03	0.533786	IVb03	0.428657	Va03	0.589537	Vb03	0.666702
IIIb04	0.606345	IVa04	0.659667	IVb04	0.617887	Va04	0.755926	Vb04	0.749253
IIIb05	0.573885	IVa05	0.616508	IVb05	0.620395	Va05	0.699082	Vb05	0.577783
IIIb06	0.502030	IVa06	0.455673	IVb06	0.512223	Va06	0.517330	Vb06	0.360505
IIIb07	0.240794	IVa07	0.353329	IVb07	0.450464	Va07	0.348625	Vb07	0.319240
IIIb08	0.366636	IVa08	0.373203	IVb08	0.365019	Va08	0.394147	Vb08	0.362880
IIIb09	0.346722	IVa09	0.325544	IVb09	0.342588	Va09	0.413304	Vb09	0.369319
IIIb10	0.338424	IVa10	0.280444	IVb10	0.315635	Va10	0.340107	Vb10	0.299117
IIIb11	0.269868	IVa11	0.195837	IVb11	0.246923	Va11	0.282495	Vb11	0.211660
IIIb12	0.193818	IVa12	0.126059	IVb12	0.177008	Va12	0.170912	Vb12	0.132062
IIIb13	0.108192	IVa13	0.065793	IVb13	0.084872	Va13	0.113072	Vb13	0.078503
IIIb14	0.069318	IVa14	0.036905	IVb14	0.053213	Va14	0.070683	Vb14	0.048276
IIIb15	0.047291	IVa15	0.032225	IVb15	0.033833	Va15	0.044225	Vb15	0.031164
IIIb16	0.039248	IVa16	0.024519	IVb16	0.029188	Va16	0.025735	Vb16	0.027044
IIIb17	0.032558	IVa17	0.023298	IVb17	0.025034	Va17	0.025609	Vb17	0.023483
IIIb18	0.031312	IVa18	0.021779	IVb18	0.021938	Va18	0.022267	Vb18	0.021354
IIIb19	0.023514	IVa19	0.021651	IVb19	0.020785	Va19	0.021763	Vb19	0.021376
IIIb20	0.025059	IVa20	0.017377	IVb20	0.017943	Va20	0.020536	Vb20	0.021176
IIIb21	0.025014	IVa21	0.018998	IVb21	0.018652	Va21	0.020812	Vb21	0.020904
IIIb22	0.024592	IVa22	0.019174	IVb22	0.019126	Va22	0.020245	Vb22	0.020036
IIIb23	0.021634	IVa23	0.018601	IVb23	0.019617	Va23	0.019762	Vb23	0.018447
IIIb24	0.021390	IVa24	0.019358	IVb24	0.019050	Va24	0.019528	Vb24	0.020968
IIIb25	0.021382	IVa25	0.017646	IVb25	0.018522	Va25	0.018580	Vb25	0.019338
IIIb26	0.021325	IVa26	0.018550	IVb26	0.017599	Va26	0.019044	Vb26	0.019854
IIIb27	0.021415	IVa27	0.017950	IVb27	0.018555	Va27	0.018489	Vb27	0.019439
IIIb28	0.019547	IVa28	0.017980	IVb28	0.019095	Va28	0.018125	Vb28	0.018780
IIIb29	0.020207	IVa29	0.018148	IVb29	0.017251	Va29	0.019396	Vb29	0.018183
IIIb30	0.019367	IVa30	0.017446	IVb30	0.018684	Va30	0.018701	Vb30	0.019006
IIIb31	0.020384	IVa31	0.018246	IVb31	0.017844	Va31	0.017974	Vb31	0.018980
IIIb32	0.020104	IVa32	0.017129	IVb32	0.018064	Va32	0.018217	Vb32	0.018365
IIIb33	0.018766	IVa33	0.016917	IVb33	0.016997	Va33	0.018289	Vb33	0.018410
IIIb34	0.018907	IVa34	0.018108	IVb34	0.017332	Va34	0.017192	Vb34	0.018744
IIIb35	0.019569	IVa35	0.015870	IVb35	0.016933	Va35	0.017297	Vb35	0.019083
IIIb36	0.018289	IVa36	0.016544	IVb36	0.017547	Va36	0.017483	Vb36	0.017987
IIIb37	0.018517	IVa37	0.017389	IVb37	0.016005	Va37	0.017306	Vb37	0.017718
IIIb38	0.017835	IVa38	0.017634	IVb38	0.016253	Va38	0.016990	Vb38	0.017506
IIIb39	0.016895	IVa39	0.015897	IVb39	0.016910	Va39	0.017199	Vb39	0.017285
IIIb40	0.017500	IVa40	0.015874	IVb40	0.016868	Va40	0.015360	Vb40	0.017672
IIIb41	0.017232	IVa41	0.015979	IVb41	0.016377	Va41	0.016127	Vb41	0.016265
IIIb42	0.015898	IVa42	0.015920	IVb42	0.015524	Va42	0.015714	Vb42	0.016382

.....continued on the next page

TABLE 2. (Continued)

Plate ID	Slope	Plate ID	Slope	Plate ID	Slope	Plate ID	Slope	Plate ID	Slope
IIIb43	0.016126	IVa43	0.014836	IVb43	0.016518	Va43	0.016320	Vb43	0.016298
IIIb44	0.016219	IVa44	0.015317	IVb44	0.015655	Va44	0.015207	Vb44	0.015805
IIIb45	0.015589	IVa45	0.015275	IVb45	0.014910	Va45	0.015381	Vb45	0.014409
IIIb46	0.014447	IVa46	0.014800	IVb46	0.015107	Va46	0.014399	Vb46	0.015424
IIIb47	0.014327	IVa47	0.014233	IVb47	0.014689	Va47	0.014807	Vb47	0.013341
IIIb48	0.014082	IVa48	0.014466	IVb48	0.014226	Va48	0.014182	Vb48	0.014855
IIIb49	0.013542	IVa49	0.013215	IVb49	0.013686	Va49	0.013675	Vb49	0.013625
IIIb50	0.012124	IVa50	0.012858	IVb50	0.013690	Va50	0.013631	Vb50	0.013408
IIIb51	0.012116	IVa51	0.013022	IVb51	0.013003	Va51	0.013335	Vb51	0.013091
IIIb52	0.011957	IVa52	0.012291	IVb52	0.012997	Va52	0.013459	Vb52	0.012410
IIIb53	0.011704	IVa53	0.012705	IVb53	0.012459	Va53	0.012185	Vb53	0.012653
IIIb54	0.010400	IVa54	0.011766	IVb54	0.012274	Va54	0.012607	Vb54	0.011328
IIIb55	0.010434	IVa55	0.011675	IVb55	0.011546	Va55	0.011765	Vb55	0.011651
IIIb56	0.009265	IVa56	0.011006	IVb56	0.011304	Va56	0.011130	Vb56	0.011766
IIIb57	0.009311	IVa57	0.010136	IVb57	0.010536	Va57	0.011073	Vb57	0.010629
IIIb58	0.008688	IVa58	0.009911	IVb58	0.010448	Va58	0.010439	Vb58	0.010309
IIIb59	0.006562	IVa59	0.009132	IVb59	0.009344	Va59	0.009769	Vb59	0.009368
IIIb60	0.007467	IVa60	0.009134	IVb60	0.009424	Va60	0.009467	Vb60	0.009952
IIIb61	0.007603	IVa61	0.009088	IVb61	0.008060	Va61	0.009293	Vb61	0.009224
IIIb62	0.006276	IVa62	0.008242	IVb62	0.008801	Va62	0.008257	Vb62	0.007686
IIIb63	0.005984	IVa63	0.007229	IVb63	0.008382	Va63	0.008150	Vb63	0.008193
IIIb64	0.005599	IVa64	0.006869	IVb64	0.007043	Va64	0.008121	Vb64	0.007744
IIIb65	0.004804	IVa65	0.007254	IVb65	0.007823	Va65	0.007274	Vb65	0.006731
IIIb66	0.004293	IVa66	0.006447	IVb66	0.006708	Va66	0.006536	Vb66	0.006799
IIIb67	0.003920	IVa67	0.005880	IVb67	0.006101	Va67	0.006479	Vb67	0.006436
IIIb68	0.003665	IVa68	0.004792	IVb68	0.005538	Va68	0.006473	Vb68	0.005909
IIIb69	0.002896	IVa69	0.005263	IVb69	0.005373	Va69	0.005449	Vb69	0.005386
IIIb70	0.002616	IVa70	0.004870	IVb70	0.004654	Va70	0.005138	Vb70	0.004967
IIIb71	0.002110	IVa71	0.004137	IVb71	0.004589	Va71	0.004574	Vb71	0.004580
IIIb72	0.001341	IVa72	0.003955	IVb72	0.003997	Va72	0.004363	Vb72	0.003971
IIIb73	0.001201	IVa73	0.003544	IVb73	0.003544	Va73	0.003909	Vb73	0.003835
IIIb74	0.000817	IVa74	0.003094	IVb74	0.003149	Va74	0.003315	Vb74	0.002966
IIIb75	0.000646	IVa75	0.002686	IVb75	0.002763	Va75	0.002795	Vb75	0.002620
IIIb76	0.000443	IVa76	0.002408	IVb76	0.002251	Va76	0.002865	Vb76	0.002389
IIIb77	0.000000	IVa77	0.001811	IVb77	0.001916	Va77	0.002351	Vb77	0.002027
IIIb78	0.000000	IVa78	0.001755	IVb78	0.001682	Va78	0.002037	Vb78	0.001700
IIIb79	0.000000	IVa79	0.001431	IVb79	0.001520	Va79	0.001781	Vb79	0.001367
IIIb80	0.000000	IVa80	0.001224	IVb80	0.001337	Va80	0.001487	Vb80	0.001022
IIIb81	0.000000	IVa81	0.000757	IVb81	0.000947	Va81	0.001147	Vb81	0.000846
IIIb82	0.000000	IVa82	0.000612	IVb82	0.000452	Va82	0.000847	Vb82	0.000505
IIIb83	0.000000	IVa83	0.000251	IVb83	0.000279	Va83	0.000563	Vb83	0.000332

On the oral surface, the plates with the larger relative growth rates are again those of cohort 2 and 3 (interambulacral) and 3 and 4 (ambulacral), but some additional patterns are also revealed. The posterior set of plates, in columns I, 1, 4, V, and 5 have a larger rate of growth than the anterior plates. Gordon (1929) recognized that in the imago *E. parma* has more plates in ambulacrum III than the others, and that asymmetric growth was necessary to maintain the roughly circular outline of the animal. This anterior-posterior growth asymmetry was investigated by Beadle (1995) and later by Lawrence & Pomory (1999), but this study clearly quantifies both where and when this asymmetry arises. There are subtle indications of bilateral asymmetry as well and the pattern suggests it is in the form of directional (DA) rather than fluctuating (FA) asymmetry (Stige *et al.* 2006), at least orally (Figure 11B). Bilateral asymmetry has been shown to occur in echinoids (Lawrence *et al.* 1998; Saucède *et al.* 2006; Savriama *et al.* 2015). While the methods used here could be used to quantify bilateral asymmetry, the relatively small sample in this case is insufficient to render statistically significant results.

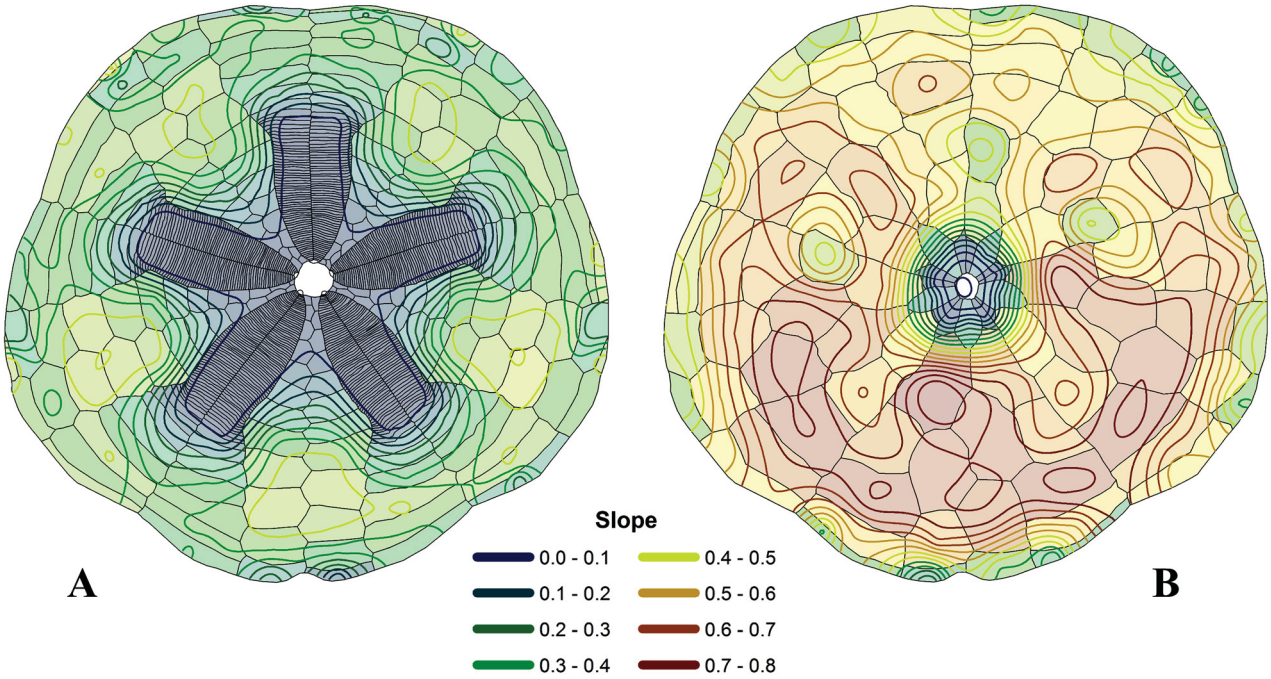

FIGURE 11. Slope of linear regressions of functions fitted to plate area (mm^2) vs. total test area (cm^2). Slopes for individual plates were posted in the centers of corresponding plates on the example plate template, gridded using a spline interpolation with barriers along the test margin, and contoured. Larger slopes indicate higher relative growth rates. Dorsal viewpoint (oral surface is mirrored). A. Aboral surface. B. Oral surface.

On the aboral surface the larger relative growth rates of the interambulacral plates in cohorts 7 and 8 form distinct growth centers between the petal tips just outside the petalodium. The enhanced growth rate of these interambulacral plates results in the indented outline of the test on the adradiad sutures that is characteristic of the species.

Plate Juxtaposition. Vertical juxtaposition of plates is a significant character for sand dollars because of interplate connection via pillars and ridges (the nomenclature for the internal structures in clypeasteroids is unsatisfactory, but its review is outside the scope of this study). The ambitus is especially significant because it defines a mirror plane of symmetry such that the growth vector of a point on the oral surface should match that of a corresponding point on the aboral surface. However, this is the case only within the region of the test with internal buttressing, growth between the oral and aboral surfaces being somewhat plastic otherwise.

A striking character of the oral interambulacral plates is that all of them are associated with internal skeletal elements (Figure 12). The basicoronal (cohort = 1) set of interambulacral plates are constrained by lantern supports (apophyses), one on each plate. The immediate post-basicoronal (cohort = 2) set of plates support the proximal ends of the interambulacral buttresses. The remaining cohorts support these buttresses plus some of the marginal pillars.

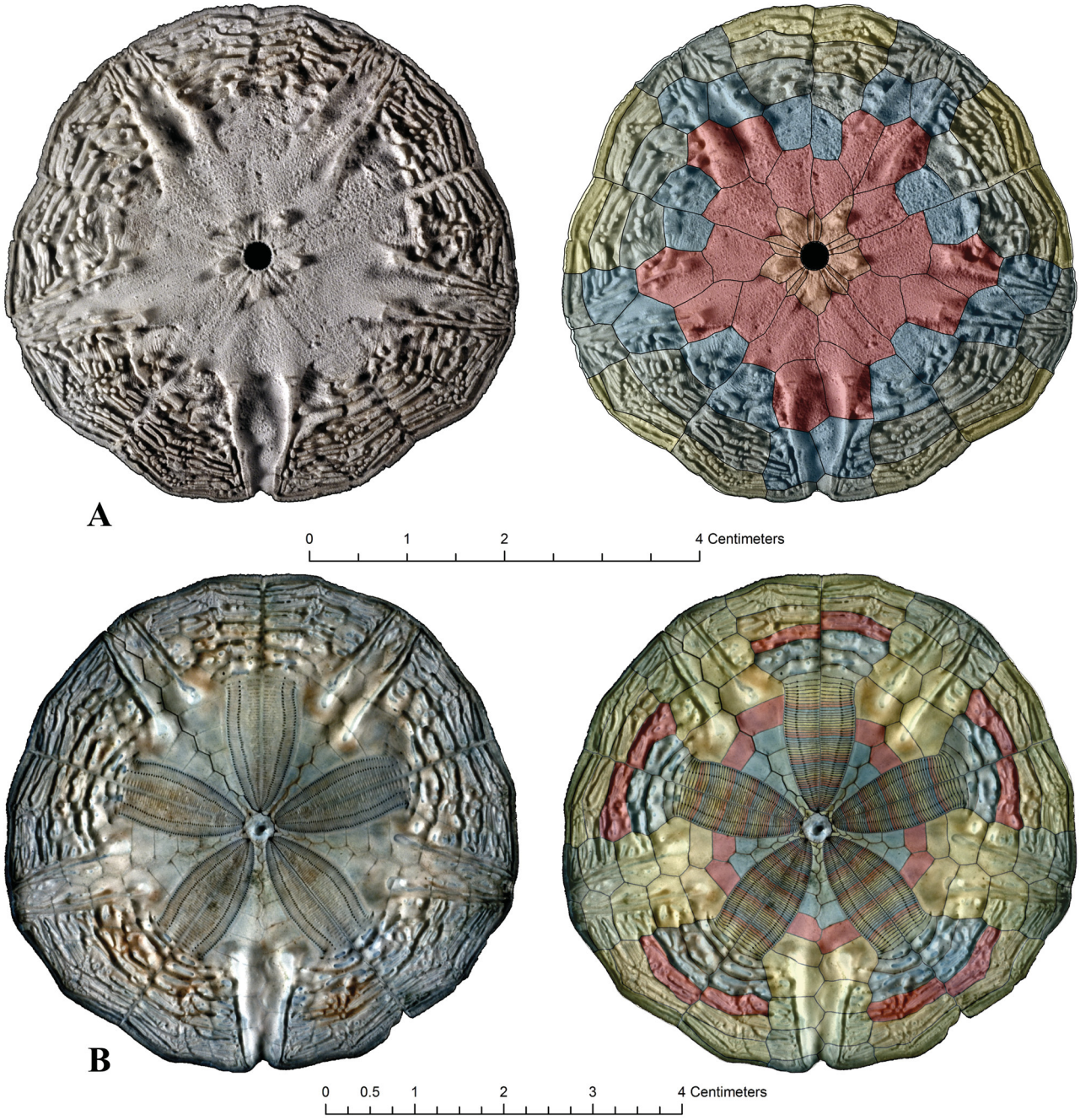

FIGURE 12. Internal views showing buttressing architecture in relation to plate cohorts. Color indicates the same plate cohort. A. Specimen length 51mm. Ambulacral cohort 1 & 2 lack buttressing structures, but all interambulacral plates contain structural elements. B. Specimen length 56mm, dorsal viewpoint (mirrored). Ambulacral plates within the petalodium lack buttressing structures, but most distal interambulacral plates are anchored by the endpoints of the interambulacral buttresses.

The size of the first cohort of ambulacral plates appears to be constrained by the geometry of the lantern, but these plates lack any auricles or flanges. The second cohort of ambulacral plates also lacks any interior structures, while the third cohort supports the first ambulacral pillars on their distal edges, and later cohorts fully support the ambulacral and marginal pillars. The aboral area of the test directly above the first 3 ambulacral cohorts is the region of plastic growth associated with the petals.

The petaloid areas can be characterized by juxtapositioning above the first 3 cohorts of ambulacral plates. This, indeed, is the driving factor in the separation between the first 2 cohorts of interambulacral plates. Most of the growth of the petals occurs in the middle region, which overlies the 2nd ambulacral cohort, and most of the

translocation occurs in the distal region, which overlies the 3rd cohort. The vertical juxtapositioning of the aboral interambulacral plates over the 2nd cohort of interambulacrals defines the extent of the petalodium.

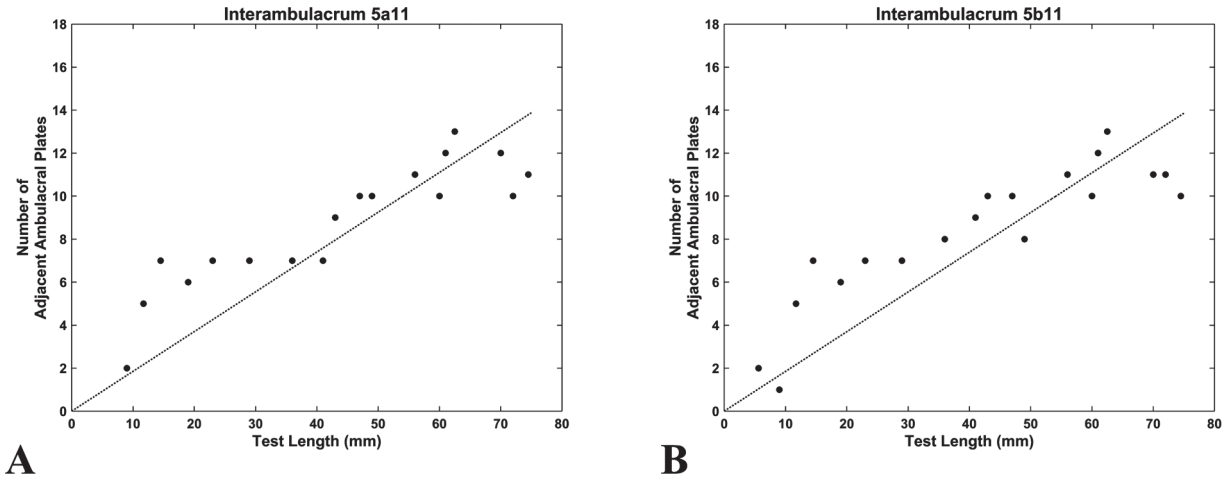

FIGURE 13. Number of ambulacral plates adjacent to an interambulacral plate vs. test length. Lines are linear fits to data points. The *y* axis is indicative of the changing A:I ratio. A. Interambulacral plate 5a, cohort 11 (adjacent plates are in column Vb). B. Interambulacral plate 5b, cohort 11 (adjacent plates are in column Ia).

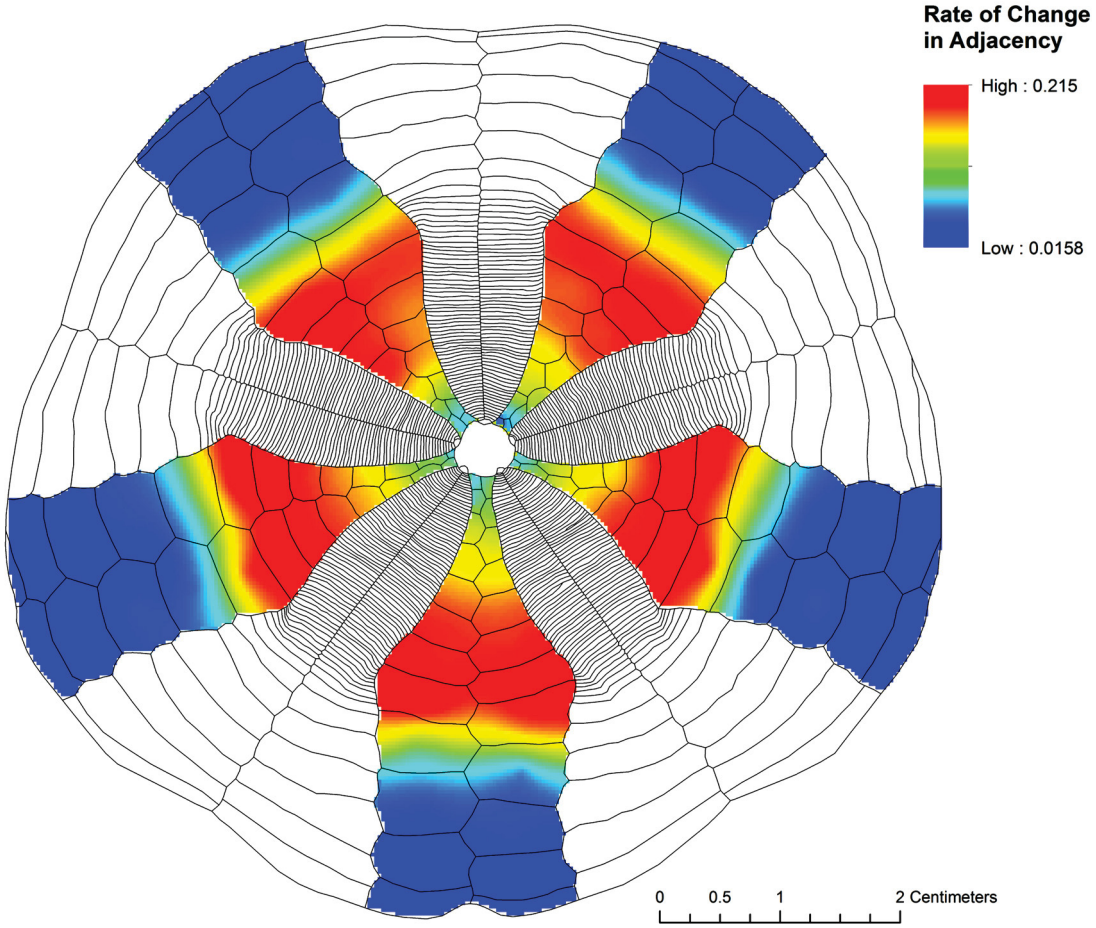

FIGURE 14. Rate of change in plate adjacency for aboral interambulacral columns measured as the slope of the linear fit to the relationship between the number of adjacent ambulacral plates and the test length (see Figure 13). Slope values for individual plates were posted in the centers of corresponding plates on the example plate template and gridded using a spline interpolation with barriers along the adradial sutures. Larger slopes indicate greater changes in plate adjacency throughout ontogeny. Plate translocation reaches a maximum near the distal ends of the petals.

Horizontal juxtaposition across the adradial suture is also a significant feature in sand dollars, differentiating between areas where the ambulacrum is petaloid from those where it is not. In particular, changes in plate juxtaposition during ontogeny show clearly that there is translocation between plates along the adradiad suture within the petalodium (Figure 13), reaching a maximum near the distal ends of the petals where plate compaction is most intense (Figure 14). In fact, the petalodium can be defined as that region within which plate juxtaposition changes significantly during ontogeny.

Logistic growth domains. The three parameters of the fitted logistic function are *K*, the maximum plate size (mm^2), *r*, the maximum rate of growth (mm^{-1}), and t_0, the proxy age (mm) at the inflection point of the sigmoidal curve. The results of the curve fitting algorithm across all of the modeled plates are somewhat noisy, for reasons noted earlier. However, when the logarithms of the parameter values are plotted against cohort number for ambulacral and interambulacral plates separately a pattern emerges (Figure 15). The pattern can be interpolated by least squares fits to polynomial equations of 4^{th} to 8^{th} order based on the log median values of the distribution. Values for *K*, *r*, and t_0 calculated from the fitting equations are given in Table 3.

TABLE 3. Logistic equation parameters. Units for *K* are maximum plate area in mm^2. Units for *r* are the proportional increase in plate area over test length in mm^{-1}. Units for t_0 are test length in mm.

	Ambulacra			Interambulacra		
Cohort	K	r	t0	K	r	t0
1	6.966994	0.064623	56.658670	14.947712	0.088583	45.266845
2	22.533499	0.062228	57.939922	62.572727	0.076766	48.492500
3	47.182927	0.061963	58.746338	81.404635	0.070546	54.333639
4	70.396438	0.063105	59.143263	55.350831	0.066504	59.654397
5	81.116372	0.065155	59.197995	38.918568	0.064140	62.068695
6	77.192038	0.067736	58.975743	37.342126	0.063929	60.722224
7	64.107411	0.070536	58.536921	43.330727	0.066478	56.504284
8	48.594847	0.073297	57.935561	46.495419	0.072126	51.265674
9	34.849812	0.075808	57.218590	39.332387	0.080522	46.815499
10	24.320434	0.077914	56.425746	28.027448	0.089954	44.457343
11	16.876268	0.079516	55.589901	20.908200	0.096851	45.117222
12	11.832375	0.080571	54.737650	18.833854	0.096712	49.709023
13	8.477975	0.081089	53.890024	17.188199	0.087260	59.344434
14	6.254634	0.081121	53.063249	9.363495	0.071411	74.809586
15	4.772092	0.080750	52.269490	2.060376	0.056049	94.163856
16	3.772576	0.080078	51.517536	0.595331	0.048251	107.926669
17	3.090098	0.079212	50.813430			
18	2.618545	0.078259	50.161007			
19	2.289784	0.077316	49.562368			
20	2.059511	0.076469	49.018268			
21	1.898367	0.075790	48.528454			
22	1.786406	0.075335	48.091935			
23	1.709671	0.075149	47.707204			
24	1.658064	0.075262	47.372422			
25	1.624038	0.075694	47.085564			
26	1.601794	0.076454	46.844534			
27	1.586808	0.077544	46.647258			
28	1.575559	0.078954	46.491755			
29	1.565374	0.080666	46.376192			

.....continued on the next page

TABLE 3. (Continued)

	Ambulacra			Interambulacra		
Cohort	K	r	t0	K	r	t0
30	1.554338	0.082656	46.298919			
31	1.541218	0.084886	46.258499			
32	1.525393	0.087315	46.253722			
33	1.506763	0.089892	46.283611			
34	1.485647	0.092558	46.347420			
35	1.462668	0.095253	46.444623			
36	1.438636	0.097914	46.574899			
37	1.414442	0.100481	46.738108			
38	1.390964	0.102901	46.934266			
39	1.368993	0.105132	47.163507			
40	1.349178	0.107146	47.426051			
41	1.331990	0.108935	47.722157			
42	1.317693	0.110511	48.052083			
43	1.306335	0.111907	48.416028			
44	1.297736	0.113181	48.814088			
45	1.291491	0.114406	49.246193			
46	1.286970	0.115678	49.712051			
47	1.283333	0.117103	50.211086			
48	1.279545	0.118799	50.742374			
49	1.274422	0.120889	51.304580			
50	1.266680	0.123496	51.895896			
51	1.255012	0.126735	52.513978			
52	1.238189	0.130702	53.155888			
53	1.215163	0.135460	53.818045			
54	1.185187	0.141012	54.496182			
55	1.147913	0.147270	55.185319			
56	1.103462	0.153997	55.879748			
57	1.052457	0.160750	56.573048			
58	0.995993	0.166804	57.258115			
59	0.935557	0.171096	57.927234			
60	0.872898	0.172226	58.572178			

Uncertainties are greatest for marginal plates (for which measurement is incomplete) and ambulacral plates of high cohort number (where minor errors in measurement have the greatest impact). The interpolated values of the parameters can be plotted by cohort number on the associated plates on the template model (Figure 16). No variation is shown within the cohorts because, unlike the earlier diagrams based on a single linear parameter, the same logistic parameter values are associated with all plates of a corresponding cohort number (only distinguishing ambulacra from interambulacra). These plots represent instantaneous growth rather than relative growth as before.

The largest *K* values are associated with the plates on the oral surface, reaching maximum values for cohort 5 ambulacral and cohort 3 interambulacral plates, corresponding to those plates which reach the largest size (Figure 15 A, B; Figure 16A). The petaloid plates have the smallest *K* values, suggesting that their size is not constrained by the sheer number of plates, but by the inherent function of growth. Interambulacral plates aborally reach a maximum *K* for the plates vertically juxtaposed above the oral cohort 2 and 3 plates, with *K* declining towards the apical system.

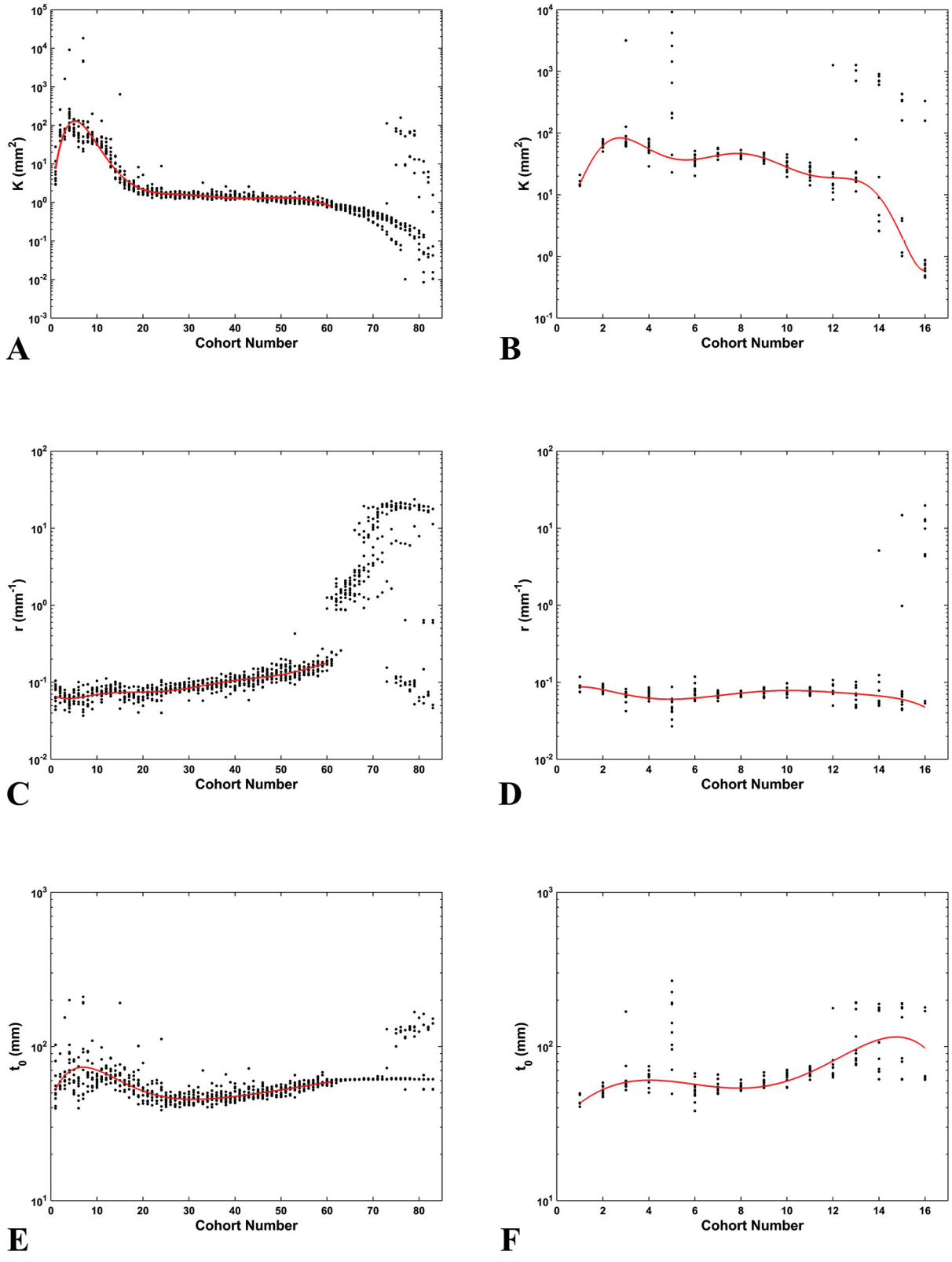

FIGURE 15. Parameters for logistic growth models plotted against cohort number. Lines indicate least squares polynomial fits to median values. A. *K* parameter (maximum size in mm^2) for ambulacral plates. B. *K* parameter for interambulacral plates. C. *r* parameter (maximum growth rate as proportional increase in plate area over test length in mm) for ambulacral plates. D. *r* parameter for interambulacral plates. E. t_0 parameter (midpoint of growth in mm) for ambulacral plates. F. t_0 parameter for interambulacral plates.

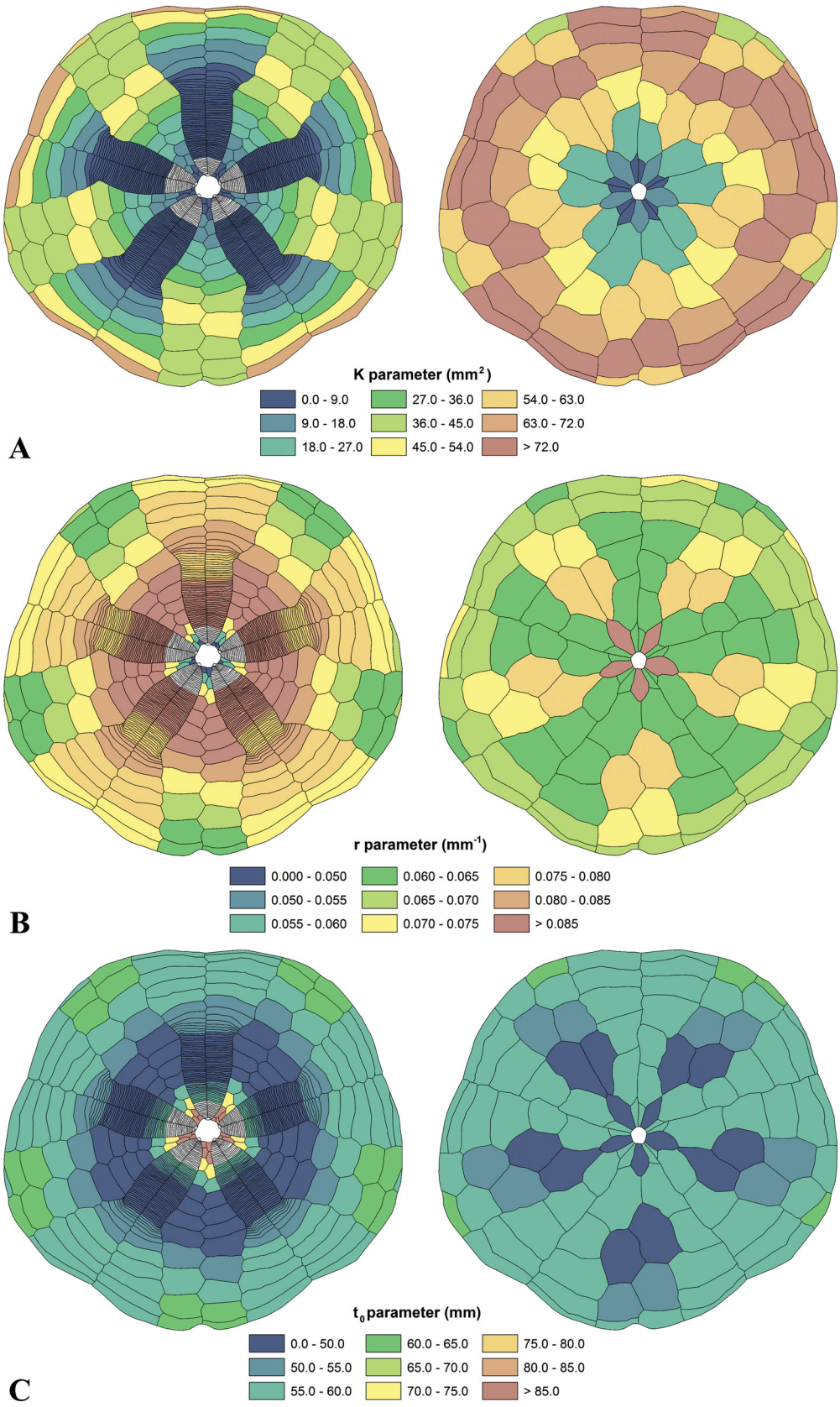

FIGURE 16. Parameters from polynomial fits to logistic growth models. Parametric values for individual plates were posted into corresponding plates on the example plate template. Dorsal viewpoint (oral surface is mirrored). A. *K* parameter. B. *r* parameter. C. t_0 parameter.

There is a narrow range of *r* values for interambulacral plates, reaching maxima in the first and second cohorts orally, and secondarily within the petalodium (Figure 15 C, D; Figure 16B). Ambulacral plates are characterized by an increasing *r* value by cohort up to about the 60th cohort, at which point the r values become chaotic. This is an artifact of very rapid growth once the plates have moved far enough from the nucleation point to overcome the geometric constraints.

The t_0 parameter increases overall with the cohort number of both ambulacral and interambulacral plates, which is expected as these plates are inserted at increasingly later times during ontogeny and thus reach their midpoint of growth at a later time (Figure 15 E, F; Figure 16C). The parameter decreases for all columns in the distal half of the petalodium before continuing to increase, indicating that in the latter stages of adult growth the proximal portions of the interambulacra continue to grow over a longer time frame than the plates in the distal portion of the petalodium. This is consistent with the results from the *r* values, namely, where plates grow faster they reach midpoint size over a shorter time frame.

Conclusions

The morphometric models improve our understanding of the growth and development of post-metamorphic *Echinarachnius parma*, in large part by expanding the description of skeletal growth to include the aboral surface and explicitly relating it to that of the oral surface. It is important to realize that the symmetry recognized from oral plate patterns continues across the ambitus and is recognizable aborally as well. The symmetry appears to originate in the larval stage, is expressed in the alternating addition of plates at the oculars, and guides the growth of the skeleton throughout the life of the animal.

The linear growth domains describe the patterns of relative growth in morphologic space, i.e., the proportion of growth distributed across the skeleton. The allometric growth between anterior and posterior oral plates compensates for the larger number of plates, derived from the rudiment, in the anterior ambulacrum III. Greater relative growth of the aboral interambulacral plates in cohorts 7 and 8 in relation to adjacent plates results in an indented outline of the test, characteristic of this and other scutelliform species.

The internal buttressing of the skeleton serves to correlate the growth of oral and aboral plates where vertically juxtaposed. A key aspect of this is the fact that all of the oral interambulacral plates are constrained by internal skeletal elements, either apophyses supporting the lantern or internal buttresses. The 2nd cohort of ambulacral plates are entirely free of internal elements and are thus the most plastic of the oral plates. The proximal ends of the interambulacral walls are anchored in the 2nd cohort of plates. This combined plasticity and anchoring results in the characteristic separation of the basicoronal and post-basicoronal interambulacral plates during ontogeny and is intimately tied to patterns of growth in the petaloid ambulacra. The extent of this plastic or unconstrained region of growth defines the petalodium of the aboral surface, which corresponds to the 1st and 2nd interambulacral plate cohorts and the 1st through 3rd ambulacral cohorts of the oral surface. Translocation of petaloid plates in relation to interambulacral plates reaches a maximum at the distal margin of the petalodium at the point where the ambulacral columns narrow before expanding to full width.

The logistic growth domains describe the patterns of growth in age (or cohort) space, i.e., the instantaneous growth functions associated with individual plates without regard to their column position. Although derived from the same underlying measurements, they grant insight into different aspects of allometric growth. The functions describing individual plate growth are intimately related to the age of a plate as represented by cohort, and thereby the sets of plates from common cohorts or ranges of cohorts define growth domains that ultimately determine the overall morphology of the coronal skeleton.

The ultimate goal of this study was to derive the baseline information required to develop a mathematical model of growth in sand dollars that could be implemented programmatically. Functions of logistic plate growth were explicitly derived, along with rates of plate addition. These are the basic parameters required in such a computational model. Quantified patterns in growth domains were also derived and can be used for validation of these models.

Acknowledgments

The author would like to thank Olaf Ellers and Amy Johnson (Bowdoin College), Rich Mooi (California Academy of Sciences), and James Sprinkle (The University of Texas at Austin) for discussions regarding aspects of this study. Comments from two anonymous reviewers substantially improved the manuscript. This research was funded in part by the Office of Research & Sponsored Programs, The University of Mississippi.

References

Beadle, S.C. (1995) Retrodisplacement of the oral and anal openings in dendrasterid sand dollars. *Evolution*, 49, 1203–1214. http://dx.doi.org/10.2307/2410445

Bertalanffy, L.v. (1938) A quantitative theory of organic growth (Inquiries on growth laws. II). *Human Biology*, 10, 181–213.

Brown, C.L. (1983) Substrate preference and test morphology of a sand dollar (*Echinarachnius parma*) population in the Gulf of Maine. *Bios*, 54, 246–254.

Cabanac, A. & Himmelman, J.H. (1996) Population structure of the sand dollar *Echinarachnius parma* in the subtidal zone of the northern Gulf of St. Lawrence, eastern Canada. *Canadian Journal of Zoology*, 74, 698–709. http://dx.doi.org/10.1139/z96-079

Cocanour, B. & Allen, K. (1967) The breeding cycles of a sand dollar and a sea urchin. *Comparative Biochemistry and Physiology*, 20, 327–331. http://dx.doi.org/10.1016/0010-406x(67)90749–9

David, B., Mooi R. & Telford, M. (1995) The ontogenetic basis of Lovén's Rule clarifies homologies of the echinoid peristome. *In:* Emson, S. C., Smith, A.B. & Campbell, A.C. (Eds.), *Echinoderm Research 1995*. A.A. Balkema, Rotterdam, pp. 155–164. http://dx.doi.org/10.1017/s0025315400031556

Deutler, F. (1926) Über das Wachstum des Seeigelskeletts. *Zoologische Jahrbücher Abteilung für Anatomie und Ontogenie der Tiere*, 48, 119–200.

Durham, J.W. (1955) Classification of clypeasteroid echinoids. *University of California Publications in Geological Sciences*, 31, 73–198.

Ebert, T.A. (2013) Growth and Survival of Postsettlement Sea Urchins. *In:* Lawrence, J.M. (Ed.), *Sea Urchins: Biology and Ecology: Developments in Aquaculture and Fisheries Science*. Elsevier, London, pp. 83–117.

Feller, W. (1940) On the logistic law of growth and its empirical verifications in biology. *Acta Biotheoretica*, 5, 51–66. http://dx.doi.org/10.1007/bf01602862

Gordon, I. (1929) Skeletal development in *Arbacia, Echinarachnius* and *Leptasterias*. *Royal Society of London, Philosophical Transactions*, series B, 217, 289–344. http://dx.doi.org/10.1098/rstb.1929.0005

Grun, T., Sievers, D. & Nebelsick, J.H. (2014) Drilling predation on the clypeasteroid echinoid *Echinocyamus pusillus* from the Mediterranean Sea (Giglio, Italy). *Historical Biology*, 26, 745–757. http://dx.doi.org/10.1080/08912963.2013.841683

Hamel, J.F. & Himmelman, J.H. (1992) Sexual dimorphism in the sand dollar *Echinarachnius parma*. *Marine Biology*, 113, 379–383. http://dx.doi.org/10.1007/bf00349162

Hyman, L.H. (1955) *The Invertebrates: Echinodermata, The Coelomate Bilateria, Volume IV*. McGraw-Hill Book Co., New York, 763 pp. http://dx.doi.org/10.1086/401699

Johnson, A.S., Salyers, J.M., Alcorn, N.J., Ellers, O. & Allen, J.D. (2013) Externally visible fluorochrome marks and allometries of growing sea urchins. *Invertebrate Biology*, 132, 251–269. http://dx.doi.org/10.1111/ivb.12024

Lang, A. (1896) *Text-Book of Comparative Anatomy*, *Volume 2*. MacMillan & Co, London, 589 pp. http://dx.doi.org/10.5962/bhl.title.23476

Lawrence, J.M. & Pomory, C.M. (1999) Eccentricity of the apical system and peristome of sand dollars (Echinodermata:Echinoidea:Clypeasteroida:Scutellina). *Gulf of Mexico Science*, 17, 35–39.

Lawrence, J.M., Pomory, C.M., Sonnenholzner, J. & Chao, C-M. (1998) Bilateral symmetry of the petals in *Mellita tenuis*, *Encope micropora*, and *Arachnoides placenta* (Echinodermata: Clypeasteroida. *Invertebrate Biology*, 117, 94–100. http://dx.doi.org/10.2307/3226855

Lohavanijaya, P. (1965) Variation in linear dimensions, test weight and ambulacral pores in the sand dollar, *Echinarachnius parma* (Lamarck). *Biological Bulletin*, 128, 401–414. http://dx.doi.org/10.2307/1539902

Lohavanijaya, P. & Swan, E.F. (1965) The separation of post-basicoronal areas from the basicoronal plates in the interambulacra of the sand dollar, *Echinarachnius parma* (Lamarck). *Biological Bulletin*, 129, 167–180.

http://dx.doi.org/10.2307/1539775
Lovén, S. (1874) Études sur les Échinoïdées. *Kongliga Svenska Vetenskaps-Akademiens Handlingar*, 11, 1–91.
http://dx.doi.org/10.5962/bhl.title.39607
Mooi, R. & David, B. (1997) Skeletal homologies of echinoderms. *In:* Waters, J.A. & Maples, C.G. (Eds.), *Geobiology of Echinoderms*, Paleontological Society Papers, Volume 3, pp. 305–335.
Moore, A.M.F. & Ellers, O. (1993) A functional morphospace, based on dimensionless numbers, for a circumferential, calcite, stabilizing structure in sand dollars. *Journal of Theoretical Biology*, 162, 253–266.
http://dx.doi.org/10.1006/jtbi.1993.1086
Nebelsick, J.H. & Kowalewski, M. (1999) Drilling predation on Recent clypeasteroid echinoids from the Red Sea. *Palaios*, 14, 127–144.
http://dx.doi.org/10.1080/08912963.2013.841683
Pianka, E.R. (2000) *Evolutionary Ecology*. Addison Wesley Educational Publishers, Inc., San Francisco, 512 pp.
Richards, F.J. (1959) A flexible growth function for empirical use. *Journal of Experimental Botany,* 10, 290–300.
http://dx.doi.org/10.1093/jxb/10.2.290
Rogers-Bennett, L., Rogers, D.W., Bennett, W.A. & Ebert, T.A. (2003) Modeling red sea urchin (*Strongylocentrotus franciscanus*) growth using six growth functions. *Fishery Bulletin*, 101, 614–626.
Saucède, T., Alibert, P., Laurin, B. & David, B. (2006) Environmental and ontogenetic constraints on developmental stability in the spatangoid sea urchin *Echinocardium* (Echinoidea). *Biological Journal of the Linnean Society*, 88, 165–177.
http://dx.doi.org/10.1111/j.1095-8312.2006.00603.x
Savriama, Y., Stige, L.C., Gerber, S., Pérez, T., Alibert, P. & David, B. (2015) Impact of sewage pollution on two species of sea urchins in the Mediterranean Sea (Cortiou, France): Radial asymmetry as a bioindicator of stress. *Ecological Indicators*, 54, 39–47.
http://dx.doi.org/10.1016/j.ecolind.2015.02.004
Seilacher, A. (1979) Constructional morphology of sand dollars. *Paleobiology*, 5, 191–221.
Seilacher, A. & Gishlick, A.D. (2015) Echinoid Construction. *In:* Seilacher, A. & Gishlick, A.D. (Eds.), *Morphodynamics*. CRC press, Boca Raton, pp. 402–428.
Sievers, D. & Nebelsick, J.H. (2014) The petalodium of clypeasteroid sand dollars: A geometric morphometric description of shape and comparison of fossil and living species [abstract]. *The Paleontological Society Special Publications*, 13, 49–50.
Smith, A.B. (2005) Growth and form in echinoids: the evolutionary interplay of plate accretion and plate addition. *In:*Briggs, D.E.G. (Ed.), *Evolving Form and Function: Fossils and Development*. Yale Peabody Museum Publications, New Haven, pp. 181–195.
Steimle, F.W. (1990) Population dynamics, growth, and production estimates for the sand dollar *Echinarachnius parma*. *Fishery Bulletin*, 88, 179–189.
Stige, L.C., David, B. & Alibert, P. (2006) On hidden heterogeneity in directional asymmetry can systematic bias be avoided? *Journal of Evolutionary Biology*, 19, 492–499.
http://dx.doi.org/10.1111/j.1420-9101.2005.01011.x
Ubisch, L.v. (1913) Die Anlage und Ausbildung des Skeletsystems einiger Echiniden und die Symmetrieverhältnisse von Larve und Imago. *Zeitschrift für Wissenschaftliche Zoologie*, 104, 119–156.
Ubisch, L.v. (1927) Über die Symmetrieverhältnisse von Larve und Imago bei regulären und irregulären Seeigeln. *Zeitschrift für Wissenschaftliche Zoologie*, 129, 541–566.
Zachos, L.G. (2009) A new computational growth model for sea urchin skeletons. *Journal of Theoretical Biology*, 259, 646–657.
http://dx.doi.org/10.1016/j.jtbi.2009.04.007
Zachos, L.G. (2015) GIS-based digital models of growth of the sand dollar *Echinarachnius parma* (Echinodermata:Echinoidea:Clypeasteroida). *MorphoBank*, Project #2276.
http://dx.doi.org/10.7934/P2276
Zachos, L.G. & Sprinkle, J. (2011) Computational model of growth and development in Paleozoic echinoids. *In:* Elewa, A.M.T. (Ed.), *Computational Paleontology*. Springer-Verlag, Berlin, pp. 75–93.